AD-A164 688 A FORTRAN PROGRAM FOR THE DETERMINATION OF UNSTEADY AIR FORCES ON GENERAL (U) AERONAUTICAL RESEARCH LABS MELBOURNE (AUSTRALIA) W WALDMAN JAN 85 ARL/STRUC-R-412 1/1

UNCLASSIFIED F/G 20/4 NL

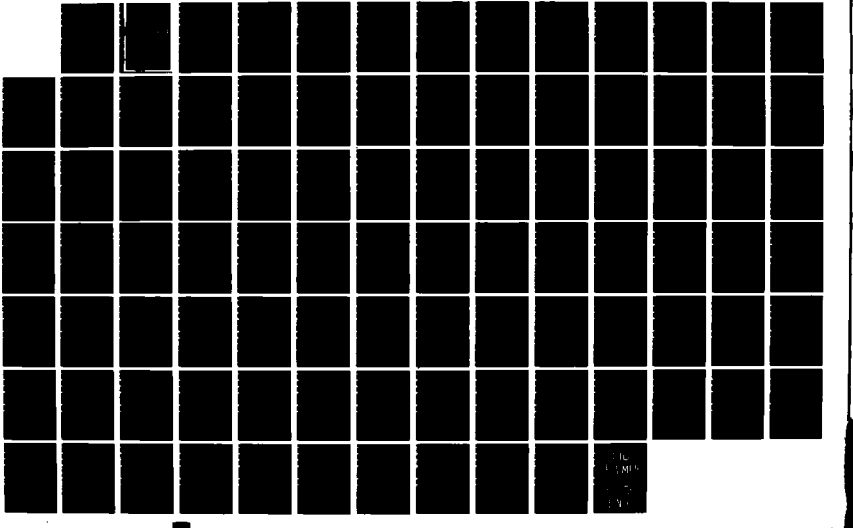

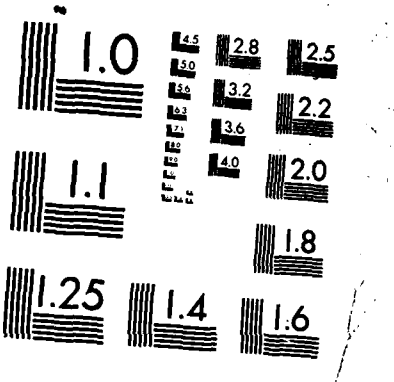

ARL-STRUC-R-412

AR-003-987

AD-A164 688

DEPARTMENT OF DEFENCE

DEFENCE SCIENCE AND TECHNOLOGY ORGANISATION

AERONAUTICAL RESEARCH LABORATORIES

MELBOURNE, VICTORIA

STRUCTURES REPORT 412

A FORTRAN PROGRAM FOR THE DETERMINATION OF UNSTEADY AIRFORCES ON GENERAL COMBINATIONS OF INTERFERING LIFTING SURFACES OSCILLATING IN SUBSONIC FLOW

W. WALDMAN

Approved for Public Release

JANUARY 1985

AR-003-987

DEPARTMENT OF DEFENCE
DEFENCE SCIENCE AND TECHNOLOGY ORGANISATION
AERONAUTICAL RESEARCH LABORATORIES

STRUCTURES REPORT 412

A FORTRAN PROGRAM FOR THE DETERMINATION OF UNSTEADY AIRFORCES ON GENERAL COMBINATIONS OF INTERFERING LIFTING SURFACES OSCILLATING IN SUBSONIC FLOW

by

W. WALDMAN

SUMMARY

A modification of the doublet lattice method of Albano and Rodden [Ref. 1] has been programmed to calculate the unsteady generalised airforces and pressures acting on interfering lifting surfaces in subsonic flow. The present method is applicable to general nonplanar and nonparallel lifting surfaces, which may be both intersecting and nonintersecting in nature. The relevant theory is developed in detail and an outline of the program and its usage is given. Comparisons with the results of other workers are included.

POSTAL ADDRESS: Director, Aeronautical Research Laboratories,
Box 4331, P.O., Melbourne, Victoria, 3001, Australia

CONTENTS

LIST OF SYMBOLS

A, B, C	coefficients in quadratic expression for $K_0 r^4$ defined in Equation E.3
A_i	nondimensional area of the i'th panel scaled by the square of the reference length defined in Equation 7.3
a, b, c	coefficients in quadratic expression for $D(p)$ defined in Equations C.17–C.19
a_i, b_i, c_i	coefficients of second-order Lagrangian interpolation polynomial defined in Equation C.20
a_n	n'th coefficient in Laschka's approximation defined in Equation B.7
a_r, b_r, c_r	coefficients of quadratic expression for r^2 defined in Equations A.9–A.11
a_x, a_y, a_z	defined in Equation A.6
a_1, a_2, a_3, a_4	variables used in the evaluation of A, B and C defined in Equations E.10–E.13
b_x, b_y, b_z	defined in Equation A.7
C	control point on the receiving panel
C_i	weights used in finite part integration defined in Equation D.15
c	chord
c	constant in Laschka's approximation defined in Equation B.7
c_j	mean chord of j'th panel defined in Equation 2.3
D	aerodynamic normalwash influence coefficient matrix defined in Equation 3.1
D_{ij}	element of matrix of aerodynamic normalwash influence coefficients
d_{ij}	submatrix of matrix of aerodynamic normalwash influence coefficients defined in Equation 8.2
dS	elemental area defined in Equation 2.1
f_p	nondimensional mode shape of the p'th mode defined in Equation 6.1
$G(x_1, y_1, z_1)$	numerator of Kernel function defined in Equation C.3

$G(p)$	numerator of Kernel function as a function of parameter p defined in Equation C.15
$\bar{H}_{-1}$, $\bar{H}_{-2}$	Struve functions defined in Equations 4.5 and 4.6
H	nondimensional vertical height parameter defined in Section 9.3
h	vertical separation between wing and tail defined in Section 9.1
h_{ji}	coefficients of polynomial used in finite part integration defined in Equation D.13
I_1, I_2	modified Bessel functions of the first kind defined in Equations 4.5 and 4.6
I_0, J_0	integrals used in the calculation of I_1 and I_2 defined in Equations B.5 and B.6
I_1, I_2	infinite integrals used in the calculation of the Kernel function defined in Equations 4.2 and 4.3
i	$\sqrt{-1}$
i, **j**, **k**	orthogonal unit vectors in the x, y and z directions
$\bar{K}_1$, $\bar{K}_2$	modified Bessel functions of the second kind defined in Equations 4.5 and 4.6
K	Kernel function defined in Equation 4.1
K_0	steady Kernel function defined in Equation 4.7
$K_0 r^2$	steady Kernel function factored by r^2 defined in Equation E.1
$K_0 r^4$	steady Kernel function factored by r^4 defined in Equation E.2
K_1, K_2	elements of Kernel function defined in Equation 4.1
$K_1^{(S)}$, $K_2^{(S)}$	elements of steady Kernel function defined in Equation 4.7
k	nondimensional frequency parameter, $\frac{\omega l}{U}$
l	reference length
l_j	quarter chord line of j'th panel defined in Equation 2.3
M	free stream Mach number
P	generalised force defined in Equation 7.1
p	pressure defined in Equation 2.1
p	parameter used in integration defined in Equation C.6
p_i	abscissas used in conjunction with integration weights

p_j	uniform pressure acting on the j'th panel defined in Equation 2.2
Q_{pq}	nondimensional generalised force in mode p due to pressures in mode q defined in Equation 7.2
R	parameter in Kernel function defined in Equation 4.1
r	parameter in Kernel function defined in Equation 4.1
$\mathbf{r}_{AB}(t)$	position vector of points along the doublet line of a panel as a function of nondimensional position parameter t defined in Equation A.1
T_1, T_2	elements of the steady and oscillatory Kernel functions defined in Equation 4.1
t	time
t	parametric position coordinate defined in Equation A.1
t_L, t_R	left and right zero crossings of K_0r^2 defined in Equations 5.3 and 5.4
t_0	zero crossing of K_0r^2 for the case of perpendicular surfaces defined in Equation 5.5
t_T	central turning point of K_0r^2 defined in Equations 5.3 and 5.4
t_{TL}, t_{TR}	left and right turning points of K_0r^2 for the case of perpendicular surfaces defined in Equations 5.6 and 5.7
$\Delta t_L, \Delta t_R$	defined in Equations 5.3 and 5.4
$\Delta t_{TL}, \Delta t_{TR}$	defined in Equations 5.6 and 5.7
U	free stream velocity
u_1	parameter in Kernel function defined in Equation 4.1
W_i	integration weights for Gaussian quadrature modified to account for $1/r^2$ behaviour of Kernel function defined in Equation E.21
w	dimensional normalwash defined in Equation 2.1
$X_{AB}(t), Y_{AB}(t), Z_{AB}(t)$	components in **i**, **j**, **k** directions of the position vector $\mathbf{r}_{AB}(t)$ defined in Equation A.1
x, y, z	orthogonal coordinates of normalwash collocation point defined in Equation 2.1
x_0, y_0, z_0	orthogonal coordinates of sending point defined in Equation 2.1
x_1, y_1, z_1	orthogonal components of distance between receiving and sending points defined in Equation 4.1
x_A, y_A, z_A	orthogonal coordinates of point A on a doublet line defined in Equations A.2–A.4

x_B, y_B, z_B	orthogonal coordinates of point B on a doublet line defined in Equations A.2–A.4
$\bar{x}, \bar{y}, \bar{z}$	defined in Equations C.7–C.9
$\tilde{x}, \tilde{y}, \tilde{z}$	defined in Equations C.7–C.9
$\hat{x}, \hat{y}, \hat{z}$	defined in Equation H.6
Z_p	displacement normal to the surface in the p'th mode defined in Equation 6.1
α	nondimensional normalwash vector defined in Equation 3.1
α'	real part of nondimensional normalwash defined in Equation 6.4
α''	imaginary part of nondimensional normalwash factored by $1/k$ defined in Equation 6.4
β	$\sqrt{1-M^2}$ defined in Equation 4.1
β_j	sweep angle of quarter chord line of j'th panel defined in Equation 2.3
γ_r, γ_s	dihedral angles of the receiving and sending panels defined in Equation 4.1
ϵ	dihedral angle of the line from point A on the sending panel to the control point on the receiving panel defined in Equation E.25
$\delta^{(1)}, \delta^{(2)}, \delta^{(3)}, \delta^{(4)}$	indicators for source and image surfaces defined in Equation 8.3
λ	nondimensional pressure function defined in Equation 2.1
λ	nondimensional horizontal separation parameter defined in Section 9.3
λ_q	nondimensional pressure due to motion in mode q defined in Equation 7.1
ν	modified frequency parameter used in Kernel function defined in Equation 4.1
ρ	density of air in the free stream
ω	circular frequency of oscillation

Subscripts and Superscripts

$^{(1)}$	indicates source group
$^{(2)}$	indicates image of source group created by reflection in the x–z plane
$^{(3)}$	indicates image of source group created by reflection in the x–z plane followed by a reflection in the x–y plane

(4)	indicates image of source group created by reflection in the x–y plane
r	receiving point or panel
s	sending point or panel
′	real component
″	imaginary component factored by $1/k$

1. INTRODUCTION

The aeroelastic stability of an aircraft is an important consideration in the overall process of determining its airworthiness. When external bodies or stores are added to the wing of an aircraft, the dynamic characteristics of the aircraft will be changed. Due to the inertial, elastic and aerodynamic coupling between the wing and its stores the flutter speed of the aircraft may be adversely affected. The aerodynamic coupling may be particularly important if the stores have aerodynamic surfaces, such as fins, that can generate large oscillatory aerodynamic forces.

At ARL there are a number of computer programs which predict unsteady aerodynamic forces acting on oscillating lifting surfaces. These programs, which are based on the doublet lattice method of Albano and Rodden [Ref. 1], are described in Reference 2 and have been optimised for simple interfering wing–tail–fin and control surface cases. They are not applicable to general combinations of interfering lifting surfaces.

Thus a requirement exists for a computer program that can calculate unsteady aerodynamic forces for general configurations of interfering lifting surfaces, including a capability for dealing with store aerodynamics. Since the doublet lattice method is readily applicable to interfering and nonplanar lifting surfaces, it is used as the basis of a program capable of dealing with general configurations. The doublet lattice method is versatile and there are essentially no restrictions on the configurations that can be handled as long as an appropriate idealisation can be developed.

2. THE DOUBLET LATTICE METHOD

This report is primarily concerned with the unsteady aerodynamic forces generated by the oscillatory motion of a lifting surface. The surface is idealised as a thin flat plate oscillating in a potential flow. The steady forces associated with the thickness and camber of the lifting surface are not considered.

The pressure difference which exists between the upper and lower surfaces of the plate is integrated to give the aerodynamic forces of interest. This oscillatory pressure is calculated by replacing the lifting surface by a planar array of unsteady pressure doublets which have strengths that are chosen such that the boundary condition of tangential flow is satisfied. The doublet strengths are related to the induced normalwash by an integral equation which for general combinations of lifting surfaces must be solved by approximate numerical methods.

In Reference 1 Albano and Rodden give the linearised integral equation relating the induced oscillatory normalwash $w(x, y, z)e^{i\omega t}$ to the pressure distribution $p(x_0, y_0, z_0)e^{i\omega t}$ over all lifting surfaces L.S. as:

$$\frac{w(x, y, z)}{U} = \frac{1}{4\pi\rho U^2} \barint\!\!\!\barint_{\text{L.S.}} K(x-x_0, y-y_0, z-z_0;\ M, \omega)p(x_0, y_0, z_0)dS \qquad 2.1$$

where K is the subsonic nonplanar Kernel function, which is a function only of geometry, Mach number M, and frequency ω. The symbol $\barint\!\!\!\barint$ indicates integration in the sense of Mangler [Ref. 3]. The coordinates of the sending and receiving points are given by (x_0, y_0, z_0) and (x, y, z) respectively.

In the doublet lattice method it is assumed that the lifting surface can be approximated by segments of planes. The surface is divided into small trapezial panels with parallel sides which lie streamwise and leading and trailing edges which are some linearly varying proportion of the

local chord behind the leading edge of the surface (Fig. 1). The panels are selected such that any surface discontinuities such as control surface edges or surface intersections lie on panel edges. Also, the panels in any coplanar streamwise column are of the same width.

By assuming that the unknown pressure p is uniform over a panel, the integral of Equation 2.1 may be approximated as follows:

$$\frac{w(x, y, z)}{U} = \sum_{j} \frac{p_j}{4\pi\rho U^2} \int\!\!\int_{\text{Panel } j} K(x - x_0, y - y_0, z - z_0;\ M, \omega) dS \qquad 2.2$$

where j is an index indicating the sending panel. The integration of K in the streamwise direction is done simply by lumping the effect into a loaded line of pressure doublets at the 1/4-chord line of each panel. Hence Equation 2.2 becomes:

$$\frac{w(x, y, z)}{U} = \sum_{j} \frac{p_j}{\rho U^2} \frac{c_j \cos \beta_j}{4\pi} \int_{l_j} K(x - x_0, y - y_0, z - z_0;\ M, \omega) dl \qquad 2.3$$

where

c_j is the mean chord of the j'th panel,

β_j is the sweep angle of the 1/4-chord line of the j'th panel.

and the subscript l_j denotes that the line integral is to be carried out over the 1/4-chord line of the j'th panel. Note that for any panel $dS = c \cos \beta\, dl$.

In Equation 2.3 the normalwash boundary condition $w(x, y, z)$ is known (see Section 6) and the pressure p_j over each panel is unknown. A set of linear algebraic equations may be formed from Equation 2.3 if the normalwash is satisfied at as many points as there are panels. There is one control or receiving point per panel and the surface normalwash boundary condition is satisfied at each of these points. The control point is located at the mid-span 3/4-chord point of each panel.

3. MATRIX FORM OF DOUBLET LATTICE METHOD

As shown by Albano and Rodden [Ref. 1], the doublet lattice method reduces the integral equation of Equation 2.1 to a set of simultaneous equations. These may be written in matrix form as:

$$\{w\} = [D]\{A\} \qquad 3.1$$

where $\{w\}$ is a complex column matrix. The i'th element is,

$$w_i = \frac{w_i(x_i, y_i, z_i)}{U} \qquad 3.2$$

and w_i is the nondimensional normalwash at the mid-span 3/4-chord point, (x_i, y_i, z_i), of the i'th panel;

$[D]$ is a complex square matrix of aerodynamic influence coefficients. The element in the i'th row and j'th column is,

$$D_{ij} = \frac{c_j \cos \beta_j}{4\pi} \int_{l_j} K_{ij}\, dl \qquad 3.3$$

and D_{ij} is the line integral of the Kernel function along the 1/4-chord line, l_j, of the j'th panel;

$\{\lambda\}$ is a complex column matrix. The j'th element is,

$$\lambda_j = \frac{p_j}{\rho U^2} \tag{3.4}$$

and λ_j is the nondimensional pressure acting uniformly over the j'th panel;

c_j is the mean chord of the j'th panel;

β_j is the sweep angle of the 1/4-chord line of the j'th panel;

K_{ij} is the subsonic nonplanar Kernel function relating the normalwash at the control point on the i'th panel to the pressure occurring over the j'th panel.

4. EVALUATION OF THE KERNEL FUNCTION

4.1 Expression for the Oscillatory Kernel Function

In Reference 4, Landahl has shown that the oscillatory subsonic nonplanar Kernel function K, which relates the complex normalwash $w(x, y, z)e^{i\omega t}$ to the complex pressure $p(x_0, y_0, z_0)e^{i\omega t}$, can be written in the following form:

$$K = e^{-i\omega x_1/U}(K_1 T_1 + K_2 T_2)/r^2 \tag{4.1}$$

where

$$T_1 = \cos(\gamma_r - \gamma_s)$$

$$T_2 = \{z_1 \cos\gamma_r - y_1 \sin\gamma_r\}\{z_1 \cos\gamma_s - y_1 \sin\gamma_s\}/r^2$$

$$K_1 = I_1 + \frac{Mr}{R}(1+u_1^2)^{-1/2} e^{-i\nu u_1}$$

$$K_2 = -3I_2 - \frac{i\nu M^2 r^2}{R^2}(1+u_1^2)^{-1/2} e^{-i\nu u_1}$$

$$- \frac{Mr}{R}\left[(1+u_1^2)\frac{\beta^2 r^2}{R^2} + 2 + \frac{Mru_1}{R}\right](1+u_1^2)^{-3/2} e^{-i\nu u_1}$$

$$x_1 = x - x_0 \qquad y_1 = y - y_0 \qquad z_1 = z - z_0$$

$$\beta = (1-M^2)^{1/2} \qquad r = (y_1^2 + z_1^2)^{1/2} \qquad R = (x_1^2 + \beta^2 r^2)^{1/2}$$

$$\nu = \frac{\omega r}{U} \qquad u_1 = \frac{MR - x_1}{\beta^2 r}$$

and γ_r and γ_s are the dihedral angles of the receiving and sending points located at (x, y, z) and (x_0, y_0, z_0) (see Appendix A and Figure 2). The terms I_1 and I_2 represent the two infinite integrals:

$$I_1(u_1, \nu) = \int_{u_1}^{\infty} \frac{e^{-i\nu u}}{(1+u^2)^{3/2}} du \qquad 4.2$$

$$I_2(u_1, \nu) = \int_{u_1}^{\infty} \frac{e^{-i\nu u}}{(1+u^2)^{5/2}} du \qquad 4.3$$

4.2 Evaluation of I_1 and I_2

In order to evaluate the Kernel function the two infinite integrals I_1 and I_2 must be determined. Since they cannot be expressed in terms of known functions they must be evaluated numerically. Computational efficiency is a prime consideration when developing a procedure for calculating I_1 and I_2 since they will be calculated numerous times. A number of alternative procedures for evaluating I_1 and I_2 will now be described.

In Reference 1, Albano and Rodden integrate Equation 4.2 by parts to yield :

$$I_1 = \left[1 - \frac{u_1}{(1+u_1^2)^{1/2}}\right] e^{-i\nu u_1} - i\nu \int_{u_1}^{\infty} \left[1 - \frac{u}{(1+u^2)^{1/2}}\right] e^{-i\nu u} du \qquad 4.4$$

The integrand in the last term of the above equation is approximated by a three-term exponential function and the integration is performed analytically. The integral I_2 is evaluated in a similar fashion, requiring integration of Equation 4.3 by parts twice.

In Reference 2, Farrell makes use of the expansions given by Davies [Ref. 5] to express I_1 and I_2 as:

$$I_1 = -\frac{i\nu\pi}{2}\left[\bar{H}_{-1}(i\nu) + \frac{2i}{\pi}\bar{K}_1(\nu) - I_1(\nu)\right] - \int_0^{u_1} \frac{e^{-i\nu u}}{(1+u^2)^{3/2}} du \qquad 4.5$$

$$I_2 = -\frac{\pi\nu^2}{6}\left[\bar{H}_{-2}(i\nu) - \frac{2}{\pi}\bar{K}_2(\nu) + iI_2(\nu)\right] - \int_0^{u_1} \frac{e^{-i\nu u}}{(1+u^2)^{5/2}} du \qquad 4.6$$

where $\bar{H}_{-1}$ and $\bar{H}_{-2}$ are Struve functions, I_1 and I_2 are modified Bessel functions of the first kind, and $\bar{K}_1$ and $\bar{K}_2$ are modified Bessel functions of the second kind. These are evaluated by direct series summation [Ref. 6], with the asymptotic expansions being used for larger values of ν. The finite integrals of Equations 4.5 and 4.6 are evaluated by a numerical technique which divides the range of integration into a number of regions, the lengths of which are functions of ν. The integration is performed over each of these smaller regions using six-point Gaussian quadrature. For values of u_1 that are large in magnitude the expressions for I_1 and I_2 simplify considerably since many of the terms may be neglected. Although this method is more accurate than that of Reference 1, the computation time is considerably greater.

In Reference 7, Geising *et al.* improve on the method used in Reference 1 by replacing the three-term exponential approximation to the integrand of Equation 4.4 with an eleven-term exponential approximation due to Laschka [Ref. 8]. The maximum error of this approximation is 0·135% [Ref. 7], and, as before, its use allows I_1 and I_2 to be evaluated analytically. A comparison between this method and that of Reference 2 was carried out by calculating trial values of the Kernel function. Good agreement between the two approaches was noted, and the method of Reference 7 was adopted since it reduced the computation time involved in the calculation of the Kernel function, as well as yielding results of a high accuracy.

A detailed description of the method used for calculating I_1 and I_2 is to be found in Appendix B.

4.3 Expression for the Steady Kernel Function

The expression for the steady Kernel function given in Reference 9 may be written in the following form:

$$K_0 = (K_1^{(S)} T_1 + K_2^{(S)} T_2)/r^2 \qquad 4.7$$

where

$$T_1 = \cos(\gamma_r - \gamma_s)$$

$$T_2 = \{z_1 \cos\gamma_r - y_1 \sin\gamma_r\}\{z_1 \cos\gamma_s - y_1 \sin\gamma_s\}/r^2$$

$$K_1^{(S)} = 1 + \frac{x_1}{R}$$

$$K_2^{(S)} = -2 - 3\frac{x_1}{R} + \left(\frac{x_1}{R}\right)^3$$

$$= \left(\frac{x_1}{R} - 2\right)\left(\frac{x_1}{R} + 1\right)^2$$

and the other symbols are as defined in Equation 4.1. The expression for the steady Kernel is considerably simpler than that for the oscillatory Kernel function. Hence when the frequency of oscillation can be assumed to be zero it is advantageous to use Equation 4.7 in preference to Equation 4.1.

5. INTEGRATION OF THE KERNEL FUNCTION

At this point it is desirable to discuss the nonplanar Kernel function as contrasted with the planar one, since the nature of the Kernel function will have a direct bearing on the integration scheme that is adopted (see Appendices C and D).

5.1 Behaviour of the Steady Kernel Function

It is convenient to confine our investigation to the behaviour of the steady Kernel function since this function is amenable to an analytical approach. The underlying assumption of this analysis is that the salient features of the steady Kernel function are representative of the behaviour displayed by the oscillatory Kernel function.

Following the approach of Berman *et al.* [Ref. 10], Figure 3 provides a comparison of the steady nonplanar Kernel function (Equation 4.7 with $z_1 \neq 0$) and the steady planar Kernel function (Equation 4.7 with $z_1 = 0$). In Figure 3 the values of the Kernel function are plotted against the spanwise variable y_1 in the vicinity of $y_1 = 0$ for several values of vertical distance z_1 and for chordwise distance $x_1 = 1$. The chordwise variation is not shown since the nonplanar Kernel function is very similar to the planar Kernel function for the x_1 coordinate [Ref. 10].

The figure clearly shows that the spanwise variation of the nonplanar Kernel function in the vicinity of the control-point station is very different from that of the planar Kernel function. The singularity at $y_1 = 0$ is no longer present. Instead, a sharp reversal in the trend of the Kernel function is experienced, resulting in a large negative, but finite, value at $y_1 = 0$. Thus the Mangler concept [Ref. 3] of the "finite part of infinite integrals" (cf. Section 2) is no longer required for the integration of the nonplanar Kernel function.

In Reference 10, Berman *et al.* found that the twin positive peaks of the nonplanar Kernel function are located at $y_1 = \pm z_1\sqrt{3}$ where z_1 is the vertical separation between the nonplanar (but parallel) lifting surfaces. Since the large gradients of this Kernel function occur between these peaks, it is essential that the relatively small region $-z_1\sqrt{3} < y_1 < +z_1\sqrt{3}$ be provided with a high density of integration stations.

Although the function shown in Figure 3 is symmetric about $y_1 = 0$, this is not the case when dealing with general combinations of nonplanar nonparallel lifting surfaces. The amount of asymmetry which arises is, however, small in comparison with the symmetric part of the Kernel.

The above mentioned behaviour must be adequately accounted for in the line integral of Equation 3.2. If suitable integration schemes are not implemented then the aerodynamic influence coefficients will lose accuracy as the vertical separation between any two surfaces is reduced. Finally, at very small values of vertical separation, as $z_1 \to 0$, the results will be completely inaccurate.

The previous discussion applies to nonplanar horizontal lifting surfaces. For the general case of combinations of nonplanar nonparallel lifting surfaces it is necessary to consider the variable $r^2 = y_1^2 + z_1^2$ rather than the variable z_1 in isolation. For this general case numerical difficulties in the integration will arise when $r^2 \to 0$.

5.2 Behaviour of K_0r^2 for Nonplanar Panel Combinations

It is clear that the ill-conditioning of the integrand in Equation 3.2 presents computational difficulties. By analytically incorporating the $1/r^2$ behaviour of the Kernel function into the line integral we may write Equation 3.3 in the following form:

$$D_{ij} = \frac{c_j \cos \beta_j}{4\pi} \int_{l_j} \frac{K_1 T_1 + K_2 T_2}{r^2} e^{-i\omega x_1 U} dl \qquad 5.1$$

This has the effect of minimising the variations that must be dealt with by the integration scheme.

In order to maximise the accuracy of integration it is worthwhile examining the behaviour of the numerator of Equation 5.1 for commonly occurring situations. Once again we confine our attention to the steady Kernel function by utilising the assumptions presented in Section 5.1.

For the steady case the numerator of Equation 5.1 (neglecting $c_j \cos \beta_j/4\pi$) may be written as:

$$K_0r^2 = K_1^{(S)}T_1 + K_2^{(S)}T_2 \qquad 5.2$$

The typical behaviour of K_0r^2 is illustrated in Figure 4. Values of K_0r^2 are plotted against the spanwise variable y_1 in the vicinity of $y_1 = 0$ for three values of vertical distance z_1 and a chordwise distance $x_1 = 1$, with both the sending and receiving panels lying in planes parallel to the horizontal plane. Note that the variation in the vicinity of $y_1 = 0$ is now considerably less than that of the corresponding curves in Figure 3. Furthermore, the curves are asymptotic to the value of $+1{\cdot}0$ for values of $y_1 \to \pm\infty$, rather than zero as in Figure 3.

The occurrence of aerodynamic surfaces that are perpendicular to each other is quite common (e.g. a T-tail and the cruciform fins at the rear of a missile). For such cases the variation of K_0r^2 differs considerably from that illustrated in Figure 4. The behaviour of K_0r^2 for perpendicular surfaces is illustrated in Figure 5. It is seen that there is only one zero crossing in contrast to the two zero crossings evident in Figure 4. Also, there are only two turning points instead of three.

5.3 Prediction of Zero Crossings and Turning Points

Although the numerator of the integrand in Equation 5.1 is much better behaved than the integrand of Equation 3.2, the highly localised nature of K_0r^2 is still evident in Figures 4 and 5.

In order to maximise the accuracy of integration it is essential that the relatively small region of rapid variation be provided with a high density of integration stations. Hence it is necessary to develop procedures for determining the location of this small region and deciding whether it lies on the interval of integration l_j (defined in Equation 3.3).

Following the approach of Berman [Ref. 10] an attempt was made to derive an analytical technique for determining the turning points of K_0r^2, since these define the region of interest. This particular approach was abandoned because of its complexity. Also, the long computation times would have made any calculations relatively expensive.

A considerably simpler and more efficient method resulted when attention was focussed on the zero crossings of K_0r^2, rather than its turning points. It is possible to write x_1, y_1 and z_1 in terms of a parameter t, where the range $0 \leqslant t \leqslant 1$ represents the interval of integration l_j. Hence, for any such interval, the Kernel function may be defined as a function of t. Turning our attention to Figure 6, the left and right zero crossings, t_L and t_R, are estimated using the method described in Appendix E. The turning point, t_T, is then located by numerical subdivision of the interval between the zero crossings. Hence the two intervals, Δt_L and Δt_R, may be calculated from:

$$\Delta t_L = t_T - t_L \tag{5.3}$$

$$\Delta t_R = t_R - t_T \tag{5.4}$$

Note that Figure 4 illustrates the special case where $\Delta t_L = \Delta t_R$ and $t_T = 0{\cdot}5$, since in general $\Delta t_L \neq \Delta t_R$ and t_T does not occur in the centre of the interval l_j. From a further inspection of Figure 4 it would appear that the region of greatest variation of K_0r^2 lies approximately within the interval:

$$t_T - 6\Delta t_L < t < t_T + 6\Delta t_R \tag{5.5}$$

Hence this region should be provided with a high density of integration stations.

The above method is not valid for aerodynamic surfaces that are perpendicular to each other since only one zero crossing exists for such cases. Due to a number of simplifications that occur, it is possible to estimate the positions of the turning points for cases where the surfaces are perpendicular. Referring to Figure 7, the left and right turning points, t_{TL} and t_{TR}, are estimated using the method described in Appendix F, whereas the zero crossing, t_0, may be estimated using the method of Appendix E. Hence we may define the two left and right intervals, Δt_{TL} and Δt_{TR}, using:

$$\Delta t_{TL} = t_0 - t_{TL} \tag{5.6}$$

$$\Delta t_{TR} = t_{TR} - t_0 \tag{5.7}$$

Clearly, the region of rapid variation falls within the interval:

$$t_{TL} < t_0 < t_{TR} \tag{5.8}$$

Once again, this region should be provided with a high density of integration stations.

6. NORMALWASH AND PRESSURE DISTRIBUTIONS

In setting up a system of panels to model an actual case it is assumed that the system is capable of vibration in a number of modes of displacement. In mode p, the displacement normal to the mean position of a point (x, y, z) on the surface is taken to be $l f_p(x, y, z)$. When the system is

oscillating harmonically about its mean position, with circular frequency ω, in the mode p, the displacement normal to the surface is taken to be

$$Z_p(x, y, z, t) = l f_p(x, y, z) e^{i\omega t} \tag{6.1}$$

where l is the reference length.

Applying the boundary condition that the flow must be tangential to the surface requires the relationship between the normalwash and the modal displacement to be

$$w_p(x, y, z) e^{i\omega t} = \frac{DZ_p}{Dt} \tag{6.2}$$

This yields the following expression for the nondimensional normalwash

$$\frac{w_p(x, y, z)}{U} = \frac{\partial}{\partial(x/l)} f_p(x, y, z) + ikf_p(x, y, z) \tag{6.3}$$

$$= \alpha' + ik\alpha'' \tag{6.4}$$

where k is the frequency parameter $\omega l/U$. Thus the real part α' of the normalwash matrix $\{\alpha\}$ of Equation 4.1 contains the chordwise slopes of the displacement mode at the control point in each panel and the scaled imaginary part α'' contains the modal displacements at these points.

When the normalwash influence coefficient matrix $[D]$ has been calculated and the nondimensional normalwash $\{\alpha\}$ has been prescribed, the system of linear equations,

$$\{\alpha\} = [D]\{\lambda\},$$

defined previously in Equation 3.1, may be solved to find the nondimensional pressure $\{\lambda\}$ acting over all surfaces. Note that there are as many lifting pressure distributions as there are modes.

7. GENERALISED FORCES

For dynamical analyses of the vibration of aerodynamic surface combinations we generally apply Lagrange's equations of motion. This requires expressions for the generalised airforces that occur. These airforces act on the actual aerodynamic surfaces but within the linearised approximation we can take the pressures described above and evaluate the generalised airforces. The generalised force P_{pq} in the mode p due to oscillation in the mode q is given by

$$P_{pq} = \int_{L.S.}\int l f_p(x, y, z) \rho U^2 \lambda_q(x, y, z) dS \, e^{i\omega t}$$

$$\rho U^2 l \int_{L.S.}\int f_p(x, y, z) \lambda_q(x, y, z) dS \, e^{i\omega t}$$

$$\rho U^2 l^3 Q_{pq} e^{i\omega t} \tag{7.1}$$

where $L.S.$ represents the integral over all the lifting surfaces, f_p is the p'th nondimensional displacement mode, λ_q is the nondimensional pressure due to the q'th mode and k is the frequency parameter $\frac{\omega l}{U}$.

From Equation 7.1 the nondimensional generalised force Q_{pq} is

$$Q_{pq} = \frac{1}{l^2} \int_{L.S.} \int f_p(x, y, z) \lambda_q(x, y, z) dS \qquad 7.2$$

In the doublet lattice method, where the aerodynamic surfaces are approximated by panels and the pressure is assumed to be constant over each panel, Equation 7.2 simplifies to

$$Q_{pq} = \sum_{i=1}^{n} f_p{}^i \lambda_q{}^i A_i \qquad 7.3$$

where $f_p{}^i$ is the nondimensional displacement at the mid-span quarter-chord point of the i'th panel in the p'th mode, $\lambda_q{}^i$ is the pressure on the i'th panel due to the q'th mode, $l^2 A_i$ is the area of the i'th panel and n is the total number of panels used to model the aerodynamic surfaces. The mid-span quarter-chord point is called the lift point and is illustrated in Figure 1. Finally, we note that it is customary, for dynamical analyses, to write Q_{pq} in the form

$$Q_{pq} = Q'_{pq} + ikQ''_{pq} \qquad 7.4$$

where Q'_{pq} and Q''_{pq} are real quantities.

8. IDEALISATION OF GENERAL CONFIGURATIONS

In order to minimise the amount of time spent in developing a panel distribution to idealise a particular configuration, it is essential to use a procedure that defines the panel distribution by interpreting a concise and compact data set. Clearly, it is not desirable to have to define each panel individually as this would be very time consuming and the likelihood of errors would be high.

8.1 Definition of Lifting Surface Groups

A lifting surface group is composed of one or more panels and it is a subset or element of the idealised configuration. For our purposes it is looked upon as being the basic unit or building block which allows us to generate sequences of panels compatible with the requirements of the doublet lattice method.

A group is defined by reference to four nodes. Figure 8 illustrates the node numbering system associated with the topology of a typical group. Nodes 1 and 2 define the leading edge of the group, and nodes 3 and 4 specify the trailing edge. This node numbering convention defines the topology of the group and must be strictly adhered to. Furthermore, nodes 1 and 3 must lie on the same streamwise line. This requirement must also be satisfied by nodes 2 and 4.

It is useful to transform the trapezial group onto a square defined in a nondimensional coordinate system, wherein the coordinates of nodes 1, 2, 3 and 4 are as illustrated in Figure 9. Node 1 is taken as the origin of the nondimensional coordinate system associated with each group. The chordwise and spanwise ordinates, t_c and t_s, are positive in the directions shown. They have been nondimensionalised with respect to the local chord and total span of the group. Note that NC and NS refer to the number of chordwise rows and spanwise columns of panels pertaining to the group. To facilitate panel generation, it is necessary to provide only the non-dimensional chordwise and spanwise ordinates of the edges of panels in a particular group.

The panels within a given group are numbered 1, 2, 3, . . ., $NC*NS$ in a columnwise progression. As shown in Figure 9, the number of the panel in the I'th chordwise row and J'th spanwise column is given by the following equation:

$$\text{panel number} = (J-1)*NC+I \qquad \begin{matrix} 1 \leqslant I \leqslant NC \\ 1 \leqslant J \leqslant NS \end{matrix} \qquad 8.1$$

Note that the chordwise rows of panels do not have to be a constant proportion of the local chord across the span of the group; a linear variation is acceptable. Hence it is possible to have one or more rows of panels of constant (dimensional) chord defined within a group that is tapered. Some of the possible combinations are illustrated in Figure 10. It is also possible to define evenly spaced panels in either the chordwise or spanwise directions, or both, without having to specify the ordinates along the sides of the group.

8.2 Pressure and Normalwash

The definition of the direction of positive pressure and positive normalwash acting on a set of panels in a group is implicit in the topology of the group. Since all panels in a group share the topology of that group, the sense of positive pressure and normalwash is likewise defined. Note that the normalwash is positive in the same sense as the topology-defined positive pressure. Furthermore, the sense of positive pressure can be reversed from that defined by the topology of the group.

Figure 11 illustrates the pressure p and normalwash w acting on a panel. The pressure and normalwash are shown acting in their positive sense. As mentioned above, the topology of the panel, represented by the node numbers 1, 2, 3 and 4, echoes the topology of the group to which it belongs.

Figure 12 shows a view, looking forward, of some possible orientations of panels. The numbers 1 and 2 refer to the topology of the group from which the panels derive. The arrows normal to the surface of each panel indicate the sense of positive pressure as defined by the topology of the panel. Although no vertical or horizontal panels are shown, their characteristics are readily deduced by simply projecting the existing panels onto the desired axis.

8.3 Symmetry and Reflection Planes

The majority of applications of the doublet lattice method involve configurations with one or more planes of symmetry. The X-Z plane is a plane of symmetry for most cases; the right side of a lifting surface is the mirror image of the left side. In other cases an additional plane of symmetry (the X-Y plane) exists. For instance a lifting surface in the proximity of the ground (aircraft in ground effect) represents a configuration with two planes of symmetry.

In general, all flow conditions can be split up into symmetrical and/or antisymmetrical parts in relation to either plane of symmetry. If the configuration is symmetrical and the flow is either symmetrical or antisymmetrical then considerable savings in computational effort can be realised. These are apparent as a reduction in the number of normalwash influence coefficients that need to be calculated and stored in computer memory. This minimises the size of the system of equations that needs to be solved.

In order to make use of any possible simplifications due to symmetry or antisymmetry it is necessary to be able to create a system of image lifting surfaces by reflecting groups in the X Z and X Y planes. Consider the general case where a lifting surface configuration is made up of a source group and three additional images. This is illustrated in Figure 13. Once again the

numbers 1 and 2 refer to the topology of the group and the arrows indicate the sense of positive pressure. The superscripts (1), (2), (3) and (4) identify how the group was obtained as follows:

(1)—source group from which all images are developed;

(2)—image obtained by reflecting the source group in the X–Z plane;

(3)—image obtained by reflecting the source group in the X–Z plane followed by a reflection in the X–Y plane;

(4)—image obtained by reflecting the source group in the X–Y plane.

Note that the topology of the image groups in relation to the source group follows the convention established in Figure 12. Care must be exercised in using the image capability as anomolous configurations can arise under some conditions.

Considering the most general case of a source and three image groups, as depicted in Figure 13, the matrix equation given by Equation 3.1 can be written as:

$$\begin{Bmatrix} w^{(1)} \\ w^{(2)} \\ w^{(3)} \\ w^{(4)} \end{Bmatrix} = \begin{bmatrix} d_{11} & d_{12} & d_{13} & d_{14} \\ d_{21} & d_{22} & d_{23} & d_{24} \\ d_{31} & d_{32} & d_{33} & d_{34} \\ d_{41} & d_{42} & d_{43} & d_{44} \end{bmatrix} \begin{Bmatrix} p^{(1)} \\ p^{(2)} \\ p^{(3)} \\ p^{(4)} \end{Bmatrix} \tag{8.2}$$

where the d_{ij} are submatrices of matrix D.

For symmetric and antisymmetric cases the magnitudes of $p^{(1)}$, $p^{(2)}$, $p^{(3)}$ and $p^{(4)}$ are equal and only their phases can differ by 180° relative to $p^{(1)}$, say. Hence we may write:

$$\begin{Bmatrix} p^{(1)} \\ p^{(2)} \\ p^{(3)} \\ p^{(4)} \end{Bmatrix} = \begin{Bmatrix} \delta^{(1)} \\ \delta^{(2)} \\ \delta^{(3)} \\ \delta^{(4)} \end{Bmatrix} p^{(1)} \tag{8.3}$$

where the terms $\delta^{(i)}$ may take the following values

$$\delta^{(1)} = +1, -1$$

$$\delta^{(2)} = +1, -1, 0$$

$$\delta^{(3)} = +1, -1, 0$$

$$\delta^{(4)} = +1, -1, 0$$

Since it refers to the source group, $\delta^{(1)} \neq 0$, whereas since some image groups may not be included in a given configuration the appropriate δ terms will be zero. If $\delta^{(i)} = 1$ then the pressure is positive in the same sense as that defined by the topology of the source or image group. If $\delta^{(i)} = -1$ then the pressure is positive in the opposite sense to that defined by the topology.

By substituting Equation 8.3 into Equation 8.2 we obtain:

$$w^{(1)} = [\delta^{(1)}d_{11} + \delta^{(2)}d_{12} + \delta^{(3)}d_{13} + \delta^{(4)}d_{14}]p^{(1)} \tag{8.4}$$

Hence the pressure distributions for all of the groups have been reduced to one distribution for the source group. Thus only that part of the interaction that involves the source group needs to be considered, since the others may be readily deduced from the symmetry or antisymmetry conditions.

Whether it be symmetric, antisymmetric or asymmetric, each type of case is defined explicitly by the chosen orientation of the positive senses of pressures for the source and image groups.

The topology-defined senses are altered by the appropriate choice of values for the δ factors in Equation 8.4. An alternative interpretation is to view $\delta^{(1)}$ as an overall multiplier determining the senses of the reference source pressures $p^{(1)}$. The remaining factors $\delta^{(2)}$, $\delta^{(3)}$ and $\delta^{(4)}$ then determine whether the effects of the image surfaces are to be added to or subtracted from the source normalwash factor d_{11} in order to obtain the correct realisation of symmetry or antisymmetry.

8.4 Example of Symmetry and Reflection Planes

As an example of the concepts described in Section 8.3, let us idealise a model of a T-tail in a wind tunnel. It is assumed that the fin and the floor of the wind tunnel provide two axes of symmetry. The effects of the remaining wind tunnel boundaries are neglected. For symmetric and antisymmetric modes only two source groups need be defined, the effects of the other surfaces being obtained by the use of images. Figure 14 shows the idealisation of the T-tail where it is assumed that the senses of pressures $p_1^{(1)}$ and $p_2^{(1)}$ define the topology of the source groups.

In order to model symmetric motion of the T-tail we have that $\delta_1^{(2)} = -1$, $\delta_1^{(3)} = +1$, $\delta_1^{(4)} = -1$ (assuming that $\delta_1^{(1)} = +1$). Since the fin does not sustain a pressure difference $\delta_2^{(1)}$ and $\delta_2^{(4)}$ are both equal to zero, which means that the fin and its image do not need to be included in the analysis. Keeping in mind the fact that $p_2^{(1)} = 0$, Equation 8.4 may be written as:

$$\begin{Bmatrix} w_1^{(1)} \\ w_2^{(1)} \end{Bmatrix} = \begin{bmatrix} (+1)d_{11}+(-1)d_{12}+(+1)d_{13}+(-1)d_{14} \\ (0)d_{21}+\quad (0)d_{22}+\quad (0)d_{23}+\quad (0)d_{24} \end{bmatrix} \begin{Bmatrix} p_1^{(1)} \\ p_2^{(1)} \end{Bmatrix} \qquad 8.5$$

where the fact that $\delta_2^{(1)} = 0$ indicates that the problem may be simplified by omitting the fin from the symmetric analysis.

For the antisymmetric case Equation 8.4 becomes:

$$\begin{Bmatrix} w_1^{(1)} \\ w_2^{(1)} \end{Bmatrix} = \begin{bmatrix} (+1)d_{11}+(+1)d_{12}+(-1)d_{13}+(-1)d_{14} \\ (+1)d_{21}+\quad (0)d_{22}+\quad (0)d_{23}+(-1)d_{24} \end{bmatrix} \begin{Bmatrix} p_1^{(1)} \\ p_2^{(1)} \end{Bmatrix} \qquad 8.6$$

Hence it is seen that symmetric and antisymmetric cases can be dealt with by appropriately specifying the applicable δ factors.

9. COMPARISON WITH OTHER METHODS

In order to illustrate the method discussed above, which has been implemented at ARL into the FORTRAN computer program AIRFORTP, three particular interfering lifting surface configurations have been investigated over a range of frequency parameters, Mach numbers and variations in geometry. These configurations are described in Sections 9.1 to 9.3 and the results compared with those obtained using alternative approaches are shown in Tables 1 to 9. The primary interest is the comparison of the results from the various computational formulations of the doublet lattice method and the lifting surface results are included only as a secondary comparison.

Note that in all the Tables the generalised forces of the form Q_{pq} are presented in terms of modulus $|Q_{pq}|$ and phase $\angle Q_{pq}$. The phase angle is given in degrees and lies in the range $0 \leq \angle Q_{pq} \leq 360°$.

9.1 AGARD Horizontal Wing and Tailplane

The AGARD horizontal wing and tail combination is shown in Figure 15. This is the configuration which AGARD specified for calculation of generalised airforces and the wing and tailplane are swept-back tapered wings in close proximity. The semi-spans of the wing and tailplane are both of unit length and the reference length is taken equal to the semi-span. The origin of coordinates is at the apex of the wing.

The configuration is in a subsonic flow of free-stream Mach number $M = 0{\cdot}8$ and is oscillating with a frequency parameter k in the range 0 to 1·5 in one of two antisymmetric modes of oscillation, defined analytically by

$$f_1(x, y, z) = y(x - 2{\cdot}25 \mid y \mid - 0{\cdot}85) \qquad \text{on the wing} \qquad 9.1$$

$$= y \qquad \text{on the tail} \qquad 9.2$$

$$f_2(x, y, z) = y \mid y \mid \qquad \text{on the wing} \qquad 9.3$$

$$= (x - 3{\cdot}35)sgn(y) \qquad \text{on the tail} \qquad 9.4$$

The first mode is torsion of the wing about an axis 38% of the local chord, coupled with roll of the tail. The second is parabolic bending of the wing coupled with pitch of the tail.

The configuration with $h \neq 0$ is obtained from the configuration when the wing and tailplane are coplanar simply by translating the tailplane a distance h parallel to the z-axis.

The comparison of results obtained for the AGARD configuration is largely based on data collected and presented by Davies [Ref. 5]. Tables 1 to 4 compare the results published in Reference 5 with the results of Farrell [Ref. 2] and the present theory. The results attributed to Davies and Albano, Perkinson and Rodden [Ref. 11] are based on lifting surface methods, the remainder being based on variations of the doublet lattice method.

In the application of the present method an array of 8 panels along the semi-span and 8 panels along the chord was used for both the wing and the tailplane. These panel distributions were evenly spaced in the spanwise and chordwise directions. As a result the panels on the wing and the tail were aligned in streamwise strips.

Table 1 presents generalised airforces for two values of frequency parameter, $k = 0$ and $k = 1{\cdot}5$, for the case where the wing and tailplane are coplanar ($h = 0$). Inspection of Table 1 shows that the present method compares favourably with the results of the other doublet lattice and lifting surface methods. Particularly good agreement is obtained with the refined doublet lattice method of Kalman, Geising and Rodden [Ref. 12]. However, for $k = 1{\cdot}5$ the present method consistently over-estimates the magnitudes of the generalised forces by an average of 10·6% when compared with the results obtained by Farrell, although the calculated phase angles are in good agreement. This is in contrast to the generally good agreement obtained for $k = 0$.

Table 2 presents results for generalised airforces for the nonplanar case with $h = 0{\cdot}6$ for frequency parameters $k = 0$ and $k = 1{\cdot}5$. Once again the results for the present method agree favourably with those of other workers. Previously made comments regarding the comparison of the present method and that due to Farrell for the case where $k = 1{\cdot}5$ are equally applicable to the results in Table 2.

Table 3 compares Davies lifting surface results for $h = 0{\cdot}6$ and a range of frequency parameters from $k = 0$ to $k = 1{\cdot}5$ with results obtained by the present method. The main purpose of the comparison is to check the variation of the generalised forces with frequency parameter. The agreement between the trends predicted by the two methods is satisfactory. The variation between the results in this comparison is within the variation exhibited by the results shown in the previous Tables.

Table 4 compares Davies lifting surface results for $k = 1{\cdot}5$ and a range of vertical separations from $h = 0$ to $h = 0{\cdot}6$ with results obtained by the present method. The results for $h = 0{\cdot}01$ and $h = 0{\cdot}04$ are of particular interest since they represent a nonplanar case with a very small vertical separation between the wing and tailplane. Small vertical separations between surfaces can lead to problems with the doublet lattice method such as those discussed in Section 5.1.

Comparison of the present method with that of Davies indicates that there is good agreement in the trends predicted for the generalised airforces as the vertical separation is varied, together with an acceptable match between individual pairs of generalised forces. In the critical region of interest when h is less than 0·1 there is acceptable agreement between the two methods.

9.2 Stark's Swept and Tapered T-Tail

A swept and tapered T-tail, first analysed by Stark in Reference 13, is shown in Figure 16. A feature of this particular T-tail configuration is that at the stabiliser-fin junction the trailing edge of the stabiliser extends beyond the trailing edge of the fin. The reference length for this configuration was taken to be the stabiliser semi-span.

The T-tail is oscillating in three rigid body modes. These consist of yawing about a vertical axis through the centre of the root chord of the fin (positive nose right), sidesway (positive left) and rolling about the fin-stabiliser intersection (positive right stabiliser down). These modes may be expressed analytically as

$$f_1(x, y, z) = 3(x + 0{\cdot}15577) \quad \text{on the fin} \tag{9.5}$$

$$= 0 \quad \text{on the stabiliser} \tag{9.6}$$

$$f_2(x, y, z) = 1{\cdot}0 \quad \text{on the fin} \tag{9.7}$$

$$= 0 \quad \text{on the stabiliser} \tag{9.8}$$

$$f_3(x, y, z) = -z \quad \text{on the fin} \tag{9.9}$$

$$= y \quad \text{on the stabilizer} \tag{9.10}$$

Figure 17 shows the panel distribution used in calculating generalised airforces for Stark's T-tail. In order to highlight the panel arrangement in the vicinity of the fin-stabiliser junction only the starboard half of the stabiliser has been included. The present aerodynamic idealisation of Stark's T-tail is quite similar to that used by Kalman, Rodden and Geising [Ref. 12]. In particular, both meshes are refined in the vicinity of the fin-stabiliser junction and the tips of the stabiliser in order to improve the estimates of pressures in these regions.

In developing a suitable panel arrangement for Stark's T-tail care was taken to ensure that at the fin-stabiliser junction none of the aerodynamic panels overlapped. This feature of the panel distribution is clearly evident in Figure 17 as the spanwise lines on the fin and stabiliser meet at the fin-stabiliser junction.

If the panels at the fin-stabiliser junction overlap each other (i.e. the spanwise lines on the fin and stabiliser do not line up at the fin-stabiliser junction) it has been found that the pressure distributions in the vicinity of the junction differ from those obtained for the lined up case. Figure 18 shows plots of the chordwise variation of nondimensional pressure λ on the fin and stabiliser at the fin-stabiliser junction for mode f_1 at a frequency parameter $k = 0$ and Mach number $M = 0$. For the case where the panels were lined up at the junction the panel distribution of Fig. 17 was used. Another configuration was then investigated where the panel distribution on the stabiliser was varied from that of Fig. 17 in that the section of the chord from the trailing edge of the fifth chordwise panel to the trailing edge of the stabiliser was divided into six evenly spaced panels. Only the rear half of the pressure distribution on each surface is shown since the effect of the panel overlap was localised to this region.

Figure 18(*a*) shows that the pressures on the fin are only slightly modified by the overlap of panels at the fin-stabiliser junction. In contrast, Figure 18(*b*) shows that the overlap of panels has significantly modified the pressure distribution acting on the rear half of the stabiliser, although only two pressure points have been significantly changed.

From the above example it is evident that the panels should be made to line up at any junctions if accurate and consistent predictions of the pressure distribution are desired. For

this particular case the effect of panel overlap did not modify the generalised forces to any significant degree ; the variation was of the order of that which could be obtained by choosing a slightly different (but still lined up) panel distribution. However, for an alternative set of modes that are more sensitive to the pressures in the region of overlap, the effect could have been significant.

Table 5 presents generalised airforces calculated for zero frequency ($k = 0$) and two Mach numbers $M = 0$ and $M = 0{\cdot}8$. The generalised forces Q_{11}, Q_{21} and Q_{31} represent the yawing moment due to yaw, the sideforce due to yaw and the rolling moment due to yaw. The agreement between the results of the present method and those obtained by different workers is generally good. If we focus attention on the doublet lattice calculations of Kalman, Rodden and Geising [Ref. 12], it is seen that the generalised airforces agree well with the largest difference being in Q_{11}. This generalised force is the fin yawing moment due to yaw, and since the side force acting on the fin, Q_{21}, agrees well, this implies that while the present method and that of Reference 12 calculate the same force acting on the fin they differ in the chordwise location of the centre of pressure.

Table 6 presents generalised airforces calculated for Mach number $M = 0{\cdot}8$ and two frequency parameters, $k = 0{\cdot}6$ and $k = 0{\cdot}9$. The results obtained by Davies, Zwaan and Kalman, Rodden and Geising were obtained from Reference 12. If we look at the results for $k = 0{\cdot}6$ and $M = 0{\cdot}8$, we see that the results for the present method lie well within the range of values predicted by the other methods. However, the agreement between the magnitude of the generalised forces Q_{11} and Q_{12} calculated by Farrell and the present method is comparatively poor. These generalised forces represent the yawing moment due to yaw and sidesway, and are obtained by a chordwise weighting of the pressure distributions due to modes f_1 and f_2. Since Farrell used only four panels down the chord of the fin and stabiliser [Ref. 2], compared to nine and eleven for the present method, while the spanwise panel distributions were similar, the poorer definition of the chordwise pressure distribution thus obtained leads to quite different estimates of Q_{11} and Q_{12} calculated by the two methods. A second coarser chordwise panel distribution was used with the present method with the result that the generalised forces Q_{11} and Q_{12} were in better agreement with those obtained by Farrell. A comparison of the results is presented in Table 7 where it is seen that the agreement with the results of Farrell is improved by the use of the coarser chordwise panel distribution.

Note that the Case 2 panel distribution consisted of four panels down the chord of the fin and five panels down the chord of the stabiliser. This combination was chosen to allow the panels along the fin-stabiliser junction to line up, whereas with the panel distribution used by Farrell this would not have been possible. This feature is likely to have contributed to the difference between the Case 2 results of the present method and those of Farrell.

9.3 ONERA Horizontal Wing and Tailplane

The ONERA horizontal wing and tail combination is shown in Figure 19. In this particular example the wing and tailplane are considered to be identical rectangles of chord $c = 0{\cdot}098$ metres and semi-span $s = 0{\cdot}1515$ metres. The leading edge of the tailplane is a distance cA metres downstream of the trailing edge of the wing and the plane of the tailplane is a distance cH metres above the plane of the wing. The position of the tailplane relative to that of the wing is then characterised by the nondimensional separation parameter A and height parameter H.

In Reference 5, Davies has presented results obtained using his lifting surface method for a set of four combinations of frequency parameter and Mach number. These are given below, viz.:

M	0·30	0·45	0·65	0·80
k	0·3856	0·2436	0·1513	0·1112

The frequency parameter k is based on a reference length equal to the chord of the wing. The variation in Mach number and frequency parameter corresponds to an oscillation of almost constant angular frequency in a compressible flow of varying velocity.

The modes of oscillation that were studied consisted of four rigid body modes, namely vertical heave of the wing, vertical heave of the tailplane, nose-up pitch of the wing about its mid-chord and nose-up pitch of the tailplane about its mid-chord. These four modes can be described analytically as

$f_1(x, y, z)$	1·0	on the wing	9.11
	0	on the tailplane	9.12
$f_2(x, y, z)$	0	on the wing	9.13
	1·0	on the tailplane	9.14
$f_3(x, y, z)$	$\frac{x}{c} - \frac{1}{2}$	on the wing	9.15
	0	on the tailplane	9.16
$f_4(x, y, z)$	0	on the wing	9.17
	$\frac{x}{c}\left(\lambda + \frac{3}{2}\right)$	on the tailplane	9.18

where the origin of the coordinates is at the centre of the leading edge of the wing.

In calculations with the present method a panel distribution of ten evenly spaced chordwise panels and twelve evenly spaced spanwise panels was used for both the wing and tailplane.

From the extensive range of results obtained by Davies, which cover a range of values of λ from $\lambda = 0$ to $\lambda = \infty$ for $H = 0$ and $H = 1.8$, the nonplanar case ($H = 1.8$) with $\lambda = 2$ and $\lambda = 1.2$ were chosen to be used in calculations with the present method. For this choice the wing tailplane proximity effects would be different from those encountered for the very closely spaced AGARD wing and tailplane configuration, thus providing a somewhat different situation compared to the AGARD configuration.

Table 8 gives results for the various M k combinations as obtained by Davies and the present method for $H = 1.8$ and $\lambda = 2$. Comparison of the two methods indicates that there is generally good agreement in the magnitudes of the generalised forces, the largest relative differences occurring in the terms Q_{11} and Q_{31}. These represent induced forces and pitching moments on the wing due to oscillation of the tailplane, and as such they are more likely to vary since for this particular case they represent a second order effect.

Turning our attention to the calculated phase angles it is seen that there is good agreement at the highest Mach number, $M = 0.8$. Then, as the Mach number decreases the agreement gets progressively worse until at the lowest Mach number the difference in phase angles falls between 3 and 5 degrees. However, this is only marginally worse than the maximum difference of 1·5 degrees encountered for the highest Mach number.

Table 9 gives results as obtained by Davies and the present method for $H = 1.8$ and $\lambda = 1.2$. It is seen that the agreement in the generalised forces Q_{11} and Q_{31} has been improved compared with the results shown in Table 8. It is clear that by reducing λ the induced forces and pitching moments on the wing due to oscillation of the tailplane have increased.

10. INTERACTIVE GRAPHICS DISPLAY FACILITY

When developing a data file for the idealisation of a given configuration it is desirable to have available the capability to generate a plot of the panel distribution corresponding to the

input data. This facilitates the checking of the panel distribution for any errors, as well as permitting the visual comparison of various alternatives.

The present program incorporates the ability to generate a data file from a given panel distribution which is compatible with the PAFEC finite element package that is in common use at ARL. This file is then processed by PAFEC so that the PAFEC Interactive Graphics System (PIGS) can be used to inspect the panel distribution. PIGS provides many powerful commands that allow the user to study the panel distribution in great detail from any chosen angle. A window facility permits close inspection of junctions at the intersections of surfaces, thus these critical areas can be easily checked to ensure that panels line up correctly.

Very complex panel distributions, such as those involving multiple underwing stores with aerodynamic surfaces, can be checked with ease. This, together with the ability to obtain hard copies of any plots generated at the VDU terminal, makes PIGS an indispensable tool for the validation of panel distributions.

The inherent compatibility of a doublet lattice panel distribution with most finite element graphics packages means that the job of preparing a data file for such a package is a relatively simple task. In program AIRFORTP only one additional subroutine was required and only this subroutine would need to be modified if a finite element graphics package other than PIGS were to be used. The advantage of such an approach is that existing computer graphics systems can be utilised, thus obviating the need to develop additional programs to improve and speed up the data development and checking phases involved in defining a panel distribution.

The possibility of creating the entire panel distribution using PIGS was considered, only to be rejected for a number of reasons. Firstly, the common requirement that panels on different surfaces line up streamwise imposes significant constraints on the panel generation scheme which could lead to difficulties. Secondly, certain types of panel distributions cannot be developed easily using PIGS, since there may be many geometrical considerations that must be taken into account. The present method which utilises a data input technique tailored to the requirements of program AIRFORTP, as well as employing the graphics capabilities of PIGS, provides capable and easy to use data preparation techniques.

11. DISCUSSION

The doublet lattice method is a simple, versatile and accurate lifting surface theory which is capable of analysing aerodynamic surfaces of arbitrary planform and dihedral. Although they were not considered in this report, control surfaces, either full- or partial-span may be included. Problems of intersecting and interfering nonplanar configurations, such as a wing-pylon-store combination, a T-tail or V-tail, a wing-tail combination, etc., may be analysed.

The computer program AIRFORTP can handle most configurations provided that they are idealised within the restrictions imposed by the doublet lattice method. Hence the previous capability at ARL for analysing wing-tail-fin combinations has been significantly extended. Appendix G contains general considerations in regard to the development of panel distributions used to model any given aerodynamic configurations. Appendix H gives a description of the format of the input data file and mode generation subroutine used by program AIRFORTP. An example of an input data file and mode generation subroutine is given in Appendix I for the analysis involving Stark's T-tail configuration.

The results obtained by the present method for planar, nonplanar and intersecting lifting surface combinations have been compared with the results of different workers. The latter were obtained by both doublet lattice and lifting surface methods. The results of the present method are seen to lie within the range of results obtained by the other methods. Problems with a small vertical (non-zero) separation between streamwise columns of panels can be handled with ease up to the point where the non-zero separation is so small as to be negligible.

12. CONCLUSIONS

The doublet lattice method is readily applicable to a large class of interfering lifting surfaces. As currently programmed at ARL the method can be used for general nonplanar and nonparallel lifting surfaces, both intersecting and nonintersecting in nature. Results have been obtained for a number of configurations and comparisons of the results have been made with results obtained by other workers. The comparisons show generally good agreement.

REFERENCES

1. Albano, E., and Rodden, W. P. — A doublet lattice method for calculating lift distributions on oscillating surfaces in subsonic flows. A.I.A.A. Journal, Vol. 7, No. 2, Feb. 1969, pp. 279–285; errata, A.I.A.A. Journal, Vol. 7, No. 11, Nov. 1969, p. 2192.

2. Farrell, P. A. — FORTRAN programs for the determination of generalised airforces on interfering surfaces oscillating in subsonic flow. Aeronautical Research Laboratories, Report SM345, August 1973.

3. Mangler, K. W. — Improper integrals in theoretical aerodynamics. R.A.E. Aero. Report 2424, June 1951.

4. Landahl, M. T. — Kernel function for nonplanar oscillating surfaces in a subsonic flow. A.I.A.A. Journal, Vol. 5, No. 5, May 1967, pp. 1045–1046.

5. Davies, D. E. — Calculations of generalised airforces on two parallel lifting surfaces oscillating harmonically in subsonic flow. Aeronautical Research Council, R & M No. 3749, Sept. 1972.

6. McLachlan, N. W. — Bessel functions for engineers. 2nd Edition, Oxford University Press, 1955.

7. Geising, J. P., Kalman, T. P., and Rodden, W. P. — Subsonic unsteady aerodynamics for general configurations. Part 1, Vol. 1—Direct application of the nonplanar doublet lattice method. Technical Report AFFDL-TR-71-5, Part 1, Vol. 1, November 1971.

8. Laschka, B. — Zur Theorie der harmonisch schwingenden tragenden Fläche bei Unterschallströmung. Zeitzchrift für Flugwissenschaften, Vol. 11, No. 7, July 1963, pp. 265–292.

9. Farrell, P. A. — A program for the computation of preliminary aerodynamic data for interfering lifting surfaces in steady subsonic flow. Aeronautical Research Laboratories, Structures Note 430, September 1976.

10. Berman, J. H., Shyprykevich, P., and Smedfjeld, J. B. — Unsteady aerodynamic forces for general wing/control-surface configurations in subsonic flow. Part 1—Theoretical development. Grumman Aircraft Engineering Corporation, Report No. ADR 06-01-67.1, December 1967.

11. Albano, E., Perkinson, F., and Rodden, W. P. — Subsonic lifting-surface theory aerodynamics and flutter analysis of interfering wing/horizontal tail configurations. Air Force Flight Dynamics Laboratory, A.F.F.D.L.-TR-70-59, Wright-Patterson Airforce Base, Ohio, September 1970.

12. Kalman, T. P., Rodden, W. P., and Geising, J. P. — Application of the doublet-lattice method to nonplanar configurations in subsonic flow. J. Aircraft, Vol. 8, No. 6, June 1971, pp. 406–413.

13. Stark, V. J. E. — Aerodynamic forces on a combination of a wing and a fin oscillating in subsonic flow. S.A.A.B. Tech. Note 54, Sweden, 1964.

14. Dwight, H. B. — Tables of integrals and other mathematical data. 4th Edition, 1966, The Macmillan Company.

15. Abramowitz, M., and Stegun, I. A. — Handbook of mathematical functions with formulas, graphs and mathematical tables. 8th Edition, 1972, Dover Publications.

APPENDIX A

Definitions relating to a general combination of a sending and receiving panel

Let us consider the interaction of a receiving panel r and a sending panel s which are defined in a global axes system (X, Y, Z) as shown in Figure 2. These panels are inclined with dihedral angles defined as γ_r and γ_s. The coordinates of points A and B at either end of the doublet line on the sending panel are A : (x_A, y_A, z_A) and B : (x_B, y_B, z_B). The coordinates of the control point C on the receiving panel are C : (x, y, z).

The position vector corresponding to points along the doublet line may be written in terms of the variable t as follows :

$$\mathbf{r}_{AB}(t) = X_{AB}(t)\mathbf{i} + Y_{AB}(t)\mathbf{j} + Z_{AB}(t)\mathbf{k} \qquad 0 \leqslant t \leqslant 1 \qquad \text{A.1}$$

where

$$X_{AB}(t) = x_A + (x_B - x_A)\, t \qquad \text{A.2}$$

$$Y_{AB}(t) = y_A + (y_B - y_A)\, t \qquad \text{A.3}$$

$$Z_{AB}(t) = z_A + (z_B - z_A)\, t \qquad \text{A.4}$$

From the definitions of x_1, y_1 and z_1 in Equation 4.1 it is clear that when we calculate the line integral of Equation 3.2 the variables x_1, y_1 and z_1 may be written in the following form :

$$\begin{aligned} x_1 &= a_x + b_x t \\ y_1 &= a_y + b_y t \\ z_1 &= a_z + b_z t \end{aligned} \qquad \text{A.5}$$

where

$$a_x = x - x_A \qquad a_y = y - y_A \qquad a_z = z - z_A \qquad \text{A.6}$$

$$b_x = x_A - x_B \qquad b_y = y_A - y_B \qquad b_z = z_A - z_B \qquad \text{A.7}$$

In the equations for the Kernel function the variable r^2 is present. The equation for r^2 may be written as :

$$\begin{aligned} r^2 &= y_1^2 + z_1^2 \\ &= a_r t^2 + b_r t + c_r \end{aligned} \qquad \text{A.8}$$

where

$$a_r \quad b_y^2 + b_z^2 \qquad \text{A.9}$$

$$b_r \quad 2[a_y b_y + a_z b_z] \qquad \text{A.10}$$

$$c_r \quad a_y^2 + a_z^2 \qquad \text{A.11}$$

If the minimum value of r^2 for a given panel combination is denoted by r^2_{min}, and the location of this minimum by t_{min}, then we have that :

$$t_{min} = -b_r/2a_r \qquad \text{A.12}$$

$$r^2_{min} = c_r - \frac{b_r^2}{4a_r} \qquad \text{A.13}$$

A decision which determines the integration procedure to be used is made on the basis of the values of r^2_{min} and t_{min} obtained for a given panel combination. Due to the organisation of panels into streamwise columns, t_{min} and r^2_{min} need only be calculated for combinations of columns rather than individual combinations of panels.

APPENDIX B

Calculation of the infinite integrals I_1 and I_2

In calculating the Kernel function two infinite integrals, I_1 and I_2, occur. For completeness the expressions are repeated below:

$$I_1(u_1, \nu) = \int_{u_1}^{\infty} \frac{e^{-i\nu u}}{(1+u^2)^{3/2}} du \qquad \text{B.1}$$

$$I_2(u_1, \nu) = \int_{u_1}^{\infty} \frac{e^{-i\nu u}}{(1+u^2)^{5/2}} du \qquad \text{B.2}$$

where the symbols u_1 and ν were defined in Section 4.1.

From Reference 7, integration of I_1 by parts once and integration of $3I_2$ by parts twice leads to:

$$I_1(u_1, \nu) = e^{-i\nu u_1}\left[1 - \frac{u_1}{(1+u_1^2)^{1/2}} - i\nu I_0(u_1, \nu)\right] \qquad \text{B.3}$$

$$3I_2(u_1, \nu) = e^{-i\nu u_1}\left\{(2+i\nu u_1)\left[1 - \frac{u_1}{(1+u_1^2)^{1/2}}\right] - \frac{u_1}{(1+u_1^2)^{3/2}}\right.$$

$$\left. - i\nu I_0(u_1, \nu) + \nu^2 J_0(u_1, \nu)\right\} \qquad \text{B.4}$$

where

$$I_0(u_1, \nu) = e^{i\nu u_1}\int_{u_1}^{\infty}\left[1 - \frac{u}{(1+u^2)^{1/2}}\right]e^{-i\nu u} du \qquad \text{B.5}$$

$$J_0(u_1, \nu) = e^{i\nu u_1}\int_{u_1}^{\infty} u\left[1 - \frac{u}{(1+u^2)^{1/2}}\right]e^{-i\nu u} du \qquad \text{B.6}$$

The integrals I_0 and J_0 can be evaluated using approximations to $u(1+u^2)^{-1/2}$ developed by Laschka [Ref. 8] in an exponential form for $u \geq 0$:

$$1 - \frac{u}{(1+u^2)^{1/2}} \approx \sum_{n=1}^{11} a_n e^{-nbu} \qquad \text{B.7}$$

where $b = 0{\cdot}372$ and the a_n are given in Table 10.

The integrals I_0 and J_0 for $u_1 \geqslant 0$ then become:

$$I_0(u_1, \nu) \approx \sum_{n=1}^{11} \frac{a_n e^{-ncu_1}}{(n^2c^2+\nu^2)}(nc-i\nu) \qquad \text{B.8}$$

$$J_0(u_1, \nu) \approx \sum_{n=1}^{11} \frac{a_n e^{-ncu_1}}{(n^2c^2+\nu^2)^2}\{n^2c^2-\nu^2+ncu_1(n^2c^2+\nu^2) \qquad \text{B.9}$$

$$-i\nu[2nc+u_1(n^2c^2+\nu^2)]\}$$

Symmetry properties of the integrands of I_1 and I_2 have permitted the consideration of only non-negative arguments u_1 since, for $u_1 < 0$, we have that:

$$I_1(u_1, \nu) = 2Re\{I_1(0, \nu)\} - Re\{I_1(-u_1, \nu)\} + iI_m\{I_1(-u_1, \nu)\} \qquad \text{B.10}$$

$$I_2(u_1, \nu) = 2Re\{I_2(0, \nu)\} - Re\{I_2(-u, \nu)\} + iI_m\{I_2(-u, \nu)\} \qquad \text{B.11}$$

Hence the desired integrals I_1 and I_2 have been explicitly defined for the range of cases $u_1 \geqslant 0$ and $u_1 < 0$.

APPENDIX C

Integration procedure when $r^2 > 0$ over the integration interval

The normalwash influence coefficient relating the normalwash on the i'th panel to the pressure over the j'th panel is:

$$D_{ij} = \frac{c_j \cos \beta_j}{4\pi} \int_{l_j} K_{ij} dl \qquad \text{C.1}$$

where $r^2 < 0$ over the interval l_j. By analytically incorporating the $1/r^2$ behaviour into the integral, Equation C.1 becomes:

$$D_{ij} = \frac{c_j \cos \beta_j}{4\pi} \int_{l_j} \left[\frac{G}{r^2}\right]_{ij} dl \qquad \text{C.2}$$

where

$$G(x_1, y_1, z_1) = (K_1 T_1 + K_2 T_2) e^{-i\omega x_1 / U} \qquad \text{C.3}$$

By subdividing the interval l_j into n smaller intervals we may write:

$$D_{ij} = \frac{c_j \cos \beta_j}{4\pi} \sum_{m=1}^{n} \int_{A_m}^{B_m} \left[\frac{G}{r^2}\right]_{ij} dl \qquad \text{C.4}$$

where the line integral is evaluated over m straight line segments between points $A_m : (x_{Am}, y_{Am}, z_{Am})$ and $B_m : (x_{Bm}, y_{Bm}, z_{Bm})$. For convenience the m, i and j subscripts will be dispensed with, and so the integral of interest in Equation C.4 may be written as:

$$I = \int_A^B \frac{G}{r^2} dl \qquad \text{C.5}$$

Let the line between points $A : (x_A, y_A, z_A)$ and $B : (x_B, y_B, z_B)$ be represented by the parametric relationship:

$$\mathbf{r}_{AB}(p) \quad X_{AB}(p)\mathbf{i} + Y_{AB}(p)\mathbf{j} + Z_{AB}(p)\mathbf{k} \qquad -1 \leqslant p \leqslant +1 \qquad \text{C.6}$$

where

$$X_{AB}(p) = \bar{x} + \hat{x}p \qquad \bar{x} = (x_A + x_B)/2 \qquad \hat{x} = (x_B - x_A)/2 \qquad \text{C.7}$$

$$Y_{AB}(p) = \bar{y} + \tilde{y}p \qquad \bar{y} = (y_A + y_B)/2 \qquad \tilde{y} = (y_B - y_A)/2 \qquad \text{C.8}$$

$$Z_{AB}(p) = \bar{z} + \tilde{z}p \qquad \bar{z} = (z_A + z_B)/2 \qquad \tilde{z} = (z_B - z_A)/2 \qquad \text{C.9}$$

Equation C.5 may now be written in the form:

$$I = \int_{-1}^{+1} \frac{G(x_1(p), y_1(p), z_1(p))}{y_1(p)^2 + z_1(p)^2} \frac{dl}{dp}\, dp \qquad \text{C.10}$$

where

$$x_1(p) = x_0 - X_{AB}(p) \qquad \text{C.11}$$

$$y_1(p) = y_0 - Y_{AB}(p) \qquad \text{C.12}$$

$$z_1(p) = z_0 - Z_{AB}(p) \qquad \text{C.13}$$

and (x_0, y_0, z_0) is the location of the control point for the panel combination being considered. Now we have that:

$$\frac{dl}{dp} = (\dot{\mathbf{r}}_{AB} \cdot \dot{\mathbf{r}}_{AB})^{1/2}$$

$$= (\dot{X}_{AB}(p)^2 + \dot{Y}_{AB}(p)^2 + \dot{Z}_{AB}(p)^2)^{1/2}$$

which yields the result:

$$\frac{dl}{dp} = (\tilde{x}^2 + \tilde{y}^2 + \tilde{z}^2)^{1/2} \qquad \text{C.14}$$

By substituting Equations C.11, C.12 and C.13 into Equation C.10 we obtain:

$$I = \frac{dl}{dp} \int_{-1}^{+1} \frac{G(p)}{D(p)} dp \qquad \text{C.15}$$

where

$$D(p) = ap^2 + bp + c \qquad \text{C.16}$$

$$a = \tilde{y}^2 + \tilde{z}^2 \qquad \text{C.17}$$

$$b = -2[\tilde{y}(y_0 - \bar{y}) + \tilde{z}(z_0 - \bar{z})] \qquad \text{C.18}$$

$$c = (y_0 - \bar{y})^2 + (z_0 - \bar{z})^2 \qquad \text{C.19}$$

Now, in order to evaluate the integral in Equation C.15, let us represent $G(p)$ by a second-order Lagrangian interpolation polynomial:

$$G(p) \sum_{i=1}^{3} (a_i p^2 + b_i p + c_i) G(p_i) \qquad \text{C.20}$$

where the abscissas p_i are the zeros of the Legendre polynomial. Substituting Equation C.20 into Equation C.15 yields:

$$I = \frac{dl}{dp} \sum_{i=1}^{3} W_i \cdot G(p_i) \qquad \text{C.21}$$

where

$$W_i = a_i \int_{-1}^{+1} \frac{p^2}{D} dp + b_i \int_{-1}^{+1} \frac{p}{D} dp + c_i \int_{-1}^{+1} \frac{1}{D} dp \qquad \text{C.22}$$

From the tables of integrals presented by Dwight in Reference 14 we find the following indefinite integrals corresponding to the definite integrals in Equation C.22:

$$\int \frac{p^2}{D} dp = \frac{p}{a} - \frac{b}{2a^2} \ln |D| + \frac{b^2 - 2ac}{2a^2} \int \frac{1}{D} dp \qquad \text{C.23}$$

$$\int \frac{p}{D} dp = \frac{1}{2a} \ln D - \frac{b}{2a} \int \frac{1}{D} dp \qquad \text{C.24}$$

$$\int \frac{1}{D} dp = \begin{cases} \dfrac{2}{(4ac - b^2)^{1/2}} \tan^{-1} \dfrac{b + 2ap}{(4ac - b^2)^{1/2}}, & b^2 - 4ac < 0 \\ \dfrac{1}{(b^2 - 4ac)^{1/2}} \ln \dfrac{b + 2ap - (b^2 - 4ac)^{1/2}}{b + 2ap + (b^2 - 4ac)^{1/2}}, & b^2 - 4ac > 0 \\ \dfrac{2}{b + 2ap}, & b^2 - 4ac = 0 \end{cases} \qquad \text{C.25}$$

The coefficients a_i, b_i and c_i of Equation C.20 may be calculated from:

$$a_1 p^2 + b_1 p + c_1 = \frac{(p - p_2)(p - p_3)}{(p_1 - p_2)(p_1 - p_3)} \qquad \text{C.26}$$

$$a_2 p^2 + b_2 p + c_2 = \frac{(p - p_1)(p - p_3)}{(p_2 - p_1)(p_2 - p_3)} \qquad \text{C.27}$$

$$a_3 p^2 + b_3 p + c_3 = \frac{(p - p_1)(p - p_2)}{(p_3 - p_1)(p_3 - p_2)} \qquad \text{C.28}$$

by equating like powers of p. Thus we obtain:

$$a_1 = \frac{1}{(p_1 - p_2)(p_1 - p_3)} \qquad b_1 = -(p_2 + p_3)a_1 \qquad c_1 = p_2 p_3 a_1 \qquad \text{C.29}$$

$$a_2 = \frac{1}{(p_2 - p_1)(p_2 - p_3)} \qquad b_2 = -(p_1 + p_3)a_2 \qquad c_2 = p_1 p_3 a_2 \qquad \text{C.30}$$

$$a_3 = \frac{1}{(p_3 - p_1)(p_3 - p_2)} \qquad b_3 = -(p_1 + p_2)a_3 \qquad c_3 = p_1 p_2 a_3 \qquad \text{C.31}$$

where the abscissas p_i and coefficients a_i, b_i and c_i are presented in Table 11.

By choosing that the abscissas p_i correspond to the abscissas in the common Gaussian quadrature formula:

$$\int_{-1}^{+1} f(p)dp \approx \sum_{i=1}^{n} w_i f(p_i) \quad ,$$

it is anticipated that the integration accuracy will be maximised compared to any other choice of p_i.

Note that since r^2 is greater than or equal to zero then the determinant b^2-4ac is less than or equal to zero. Hence in Equation C.25 the integral when $b^2-4ac > 0$ is not applicable to the problem at hand and should be neglected.

APPENDIX D

Integration procedure when $r^2 \to 0$ in the centre of the integration interval

In the doublet lattice method, when the $r^2 \to 0$ singularity occurs it must do so in the centre of the interval l_j over which the line integral of Equation 3.3 is defined. Following the method of Appendix C, the interval l_j may be subdivided into n smaller intervals. Furthermore, if we assume that the singularity falls symmetrically within the k'th interval, then the normalwash influence coefficient D_{ij} may be written as:

$$D_{ij} = \frac{c_j \cos\beta_j}{4\pi}\left\{ \sum_{m=1}^{k-1} \int_{A_m}^{B_m} \left[\frac{G}{r^2}\right]_{ij} dl + \oint_{A_k}^{B_k} \left[\frac{G}{r^2}\right]_{ij} dl \right. \qquad \text{D.1}$$

$$\left. + \sum_{m=k+1}^{n} \int_{A_m}^{B_m} \left[\frac{G}{r^2}\right]_{ij} dl \right\}$$

The integrals in the first and third terms may be calculated using the method detailed in Appendix C. It now remains to derive a method for solving the finite part integral in Equation D.1. If we dispense with the subscripts then the integral of interest is:

$$I = \oint_{A}^{B} \frac{G}{r^2} dl \qquad \text{D.2}$$

Now since $r^2 \to 0$ in the centre of the interval from point A: (x_A, y_A, z_A) to point B: (x_B, y_B, z_B), the line between these two points can be represented by the parametric relationship:

$$\mathbf{r}(p) \quad x(p)\mathbf{i} + y(p)\mathbf{j} + z(p)\mathbf{k} \qquad -1 \leq p \leq +1 \qquad \text{D.3}$$

where

$$x(p) \quad \bar{x} + \tilde{x}p \qquad \tilde{x} \quad (x_B - x_A)/2 \qquad \bar{x} \quad (x_A + x_B)/2 \qquad \text{D.4}$$

$$y(p) \quad y_0 + \tilde{y}p \qquad \tilde{y} \quad (y_B - y_A)/2 \qquad \text{D.5}$$

$$z(p) \quad z_0 + \tilde{z}p \qquad \tilde{z} \quad (z_B - z_A)/2 \qquad \text{D.6}$$

and the control point is located at (x_0, y_0, z_0). Note that when $r^2 \to 0$ the control point and lift point (shown in Fig. 2) lie on the same streamwise line.

Using the above definitions of $x(p)$, $y(p)$ and $z(p)$ we obtain :

$$x_1(p) = x_0 - (\bar{x} + \tilde{x}p) \qquad \text{D.7}$$

$$y_1(p) = -\tilde{y}p \qquad \text{D.8}$$

$$z_1(p) = -\tilde{z}p \qquad \text{D.9}$$

Hence we see that $r^2 = y_1^2 + z_1^2$ is simply :

$$r^2 = (\tilde{y}^2 + \tilde{z}^2)p^2 \qquad \text{D.10}$$

and, as in Appendix C, we have that :

$$\frac{dl}{dp} = (\tilde{x}^2 + \tilde{y}^2 + \tilde{z}^2)^{1/2} \qquad \text{D.11}$$

Thus, using Equations D.7 to D.11, Equation D.2 becomes :

$$I = \frac{1}{\tilde{y}^2 + \tilde{z}^2} \frac{dl}{dp} \int_1^{+1} \frac{G(p)}{p^2} dp \qquad \text{D.12}$$

Following the method of Farrell [Ref. 2], the numerator $G(p)$ may be approximated by a polynomial of order $(n-1)$:

$$G(p) = \sum_{i=1}^{n} \sum_{j=1}^{n} h_{ji} p^{j-1} G(p_i) \qquad \text{D.13}$$

where the h_{ji} represent the coefficients of the polynomial. The abscissas p_i are the roots of the n'th order Tchebycheff polynomial of the first kind. The abscissas may be determined from the following equation [Ref. 15, p. 889]:

$$p_i = \cos \frac{(2i-1)\pi}{2n} \qquad \text{D.14}$$

By substituting Equation D.13 into Equation D.12 we obtain :

$$I = \frac{1}{\tilde{y}^2 + \tilde{z}^2} \frac{dl}{dp} \sum_{i=1}^{n} C_i G(p_i) \qquad \text{D.15}$$

where

$$C_i = \sum_{j=1}^{n} h_{ji} \int_{-1}^{+1} p^{j-3} dp. \qquad \text{D.16}$$

By equating like powers of p, the h_{ji} may be calculated from:

$$\sum_{j=1}^{n} h_{ji} p^{j-1} = \frac{\prod_{u} (p - p_u)}{\prod_{v} (p_i - p_v)} \qquad i = 1, 2, \ldots, n \qquad \text{D.17}$$

where $\prod_{u}$ is the restricted product for $u = 1, 2, \ldots, n;\ u \neq i$,

and $\prod_{v}$ is the restricted product for $v = 1, 2, \ldots, n;\ v \neq i$.

As in Reference 2, an eighth order polynomial has been chosen. This corresponds to $n = 9$, and the abscissas p_i and weights C_i have been calculated and are listed in Table 12.

APPENDIX E

Estimating the position of the zero crossings of K_0r^2

Let us consider the interaction of a receiving panel r and a sending panel s. We wish to determine estimates of the positions of the zero crossings of the numerator of Equation 5.1 for the steady case. These zero crossings will occur somewhere along the line which is colinear with the doublet line in the sending panel, and we are specifically interested in the case where they occur on the doublet line itself.

The numerator discussed above is defined as:

$$K_0r^2 = K_1^{(S)}\cos(\gamma_r-\gamma_s)+K_2^{(S)}(z_1\cos\gamma_r-y_1\sin\gamma_r)(z_1\cos\gamma_s-y_1\sin\gamma_s)/r^2 \qquad \text{E.1}$$

Multiplying through by

$$r^2 = y_1^2+z_1^2$$

we obtain:

$$K_0r^4 = K_1^{(S)}\cos(\gamma_r-\gamma_s)(y_1^2+z_1^2)+K_2^{(S)}(z_1\cos\gamma_r-y_1\sin\gamma_r)(z_1\cos\gamma_s-y_1\sin\gamma_s) \qquad \text{E.2}$$

By substituting for z_1 and y_1 using Equations A.5 to A.11 (see Appendix A) it is possible to write Equation E.2 in the following form:

$$K_0r^4 = At^2+Bt+C \qquad \text{E.3}$$

where

$$A = K_1^{(S)}[\cos(\gamma_r-\gamma_s)a_r]+K_2^{(S)}[a_2a_4] \qquad \text{E.4}$$

$$B = K_1^{(S)}[\cos(\gamma_r-\gamma_s)b_r]+K_2^{(S)}[a_1a_4+a_2a_3] \qquad \text{E.5}$$

$$C = K_1^{(S)}[\cos(\gamma_r-\gamma_s)c_r]+K_2^{(S)}[a_1a_3] \qquad \text{E.6}$$

$$a_r = b_y^2+b_z^2 \qquad \text{E.7}$$

$$b_r = 2[a_yb_y+a_zb_z] \qquad \text{E.8}$$

$$c_r = a_y^2+a_z^2 \qquad \text{E.9}$$

$$a_1 = a_z\cos\gamma_r \quad a_y\sin\gamma_r \qquad \text{E.10}$$

$$a_2 = b_z\cos\gamma_r \quad b_y\sin\gamma_r \qquad \text{E.11}$$

$$a_3 = a_z\cos\gamma_s \quad a_y\sin\gamma_s \qquad \text{E.12}$$

$$a_4 = b_z\cos\gamma_s \quad b_y\sin\gamma_s \qquad \text{E.13}$$

In the above equations it is assumed that $K_1^{(S)}$ and $K_2^{(S)}$ are constant for the panel combination under consideration.

With reference to Figure 2, the sine and cosine of the dihedral angle of the sending panel s may be expressed as:

$$\sin \gamma_s = \frac{z_B - z_A}{[(y_B - y_A)^2 + (z_B - z_A)^2]^{1/2}} \quad \text{E.14}$$

$$\cos \gamma_s = \frac{y_B - y_A}{[(y_B - y_A)^2 + (z_B - z_A)^2]^{1/2}} \quad \text{E.15}$$

By substituting

$$-b_y = (y_B - y_A)$$

and

$$-b_z = (z_B - z_A)$$

into the above expressions we obtain:

$$\sin \gamma_s = \frac{-b_z}{(b_y^2 + b_z^2)^{1/2}} \quad \text{E.16}$$

$$\cos \gamma_s = \frac{-b_y}{(b_y^2 + b_z^2)^{1/2}} \quad \text{E.17}$$

If we rewrite a_4 (see Equation E.13) in the following form:

$$a_4 = -(b_y^2 + b_z^2)^{1/2}\left[\frac{-b_z}{(b_y^2 + b_z^2)^{1/2}} \cos \gamma_s - \frac{-b_y}{(b_y^2 + b_z^2)^{1/2}} \sin \gamma_s\right] \quad \text{E.18}$$

and then substitute Equations E.16 and E.17 into Equation E.18 we see that a_4 is identically equal to zero. Hence the coefficients A, B and C of Equation E.3 become:

$$A = K_1^{(S)}[\cos(\gamma_r - \gamma_s)a_r] \quad \text{E.19}$$

$$B = K_1^{(S)}[\cos(\gamma_r - \gamma_s)b_r] + K_2^{(S)}[a_2 a_3] \quad \text{E.20}$$

$$C = K_1^{(S)}[\cos(\gamma_r - \gamma_s)c_r] + K_2^{(S)}[a_1 a_3] \quad \text{E.21}$$

Also, a_1, a_2 and a_3 can be written as:

$$a_1 = -(a_y^2 + a_z^2)^{1/2} \sin(\gamma_r - \epsilon) \quad \text{E.22}$$

$$a_2 = +(b_y^2 + b_z^2)^{1/2} \sin(\gamma_r - \gamma_s) \quad \text{E.23}$$

$$a_3 = -(a_y^2 + a_z^2)^{1/2} \sin(\gamma_s - \epsilon) \quad \text{E.24}$$

where

$$\sin \epsilon = \frac{a_z}{(a_y^2 + a_z^2)^{1/2}} \quad \text{E.25}$$

and ϵ represents the dihedral angle of the line from point A on the sending panel to the control point on the receiving panel. From this definition of ϵ it is clear that $\sin(\gamma_r - \epsilon) = 0$ when the lift point on the sending panel lies on the plane defined by the receiving panel. Similarly, $\sin(\gamma_s - \epsilon) = 0$ when the control point on the receiving panel lies on the plane defined by the lifting panel. If the latter condition coincides with the sending and receiving panels lying perpendicular to each other, then, as expected, no mutual interference occurs.

Inspection of Equation E.19 leads to the observation that there is only one zero crossing when the sending and receiving panels are perpendicular to each other. An example of such behaviour is presented in Figure 5.

The positions of the zero crossings (in terms of the parameter t) of the numerator of Equation 5.1 can be estimated by solving the following equation:

$$At^2 + Bt + C = 0 \qquad \text{E.26}$$

for the values of t.

In the above analysis it has been assumed that $K_1^{(S)}$ and $K_2^{(S)}$ may be taken to be constants over the length of the doublet line in the sending panel. This approximation is valid since both $K_1^{(S)}$ and $K_2^{(S)}$ are slowly varying functions and the interval over which they are assumed to be constant is itself quite small. More often than not, the zero crossings will occur outside the interval defined by the doublet line. In this case the assumed values of $K_1^{(S)}$ and $K_2^{(S)}$ may not be accurate, but this is unimportant since we are only interested when the zero crossings occur along the doublet line. When the zero crossings occur along the doublet line the estimate of their location may be improved by repeating the calculation using revised average values of $K_1^{(S)}$ and $K_2^{(S)}$ calculated over a smaller interval defined by the initial estimates of the zero crossings.

For critical cases where the zero crossings are close together the approximation that $K_1^{(S)}$ and $K_2^{(S)}$ are constant over the small interval is particularly good. Geising *et al.* [Ref. 7] have shown that when $r^2 \to 0$ the terms $K_1 \to 2$ and $K_2 \to -4$, where K_1 and K_2 are elements of the unsteady Kernel function given in Equation 4.1. Hence, as $r^2 \to 0$ then $K_1^{(S)} \to 2$ and $K_2^{(S)} \to -4$.

APPENDIX F

Estimating the position of the turning points of K_0r^2 for a perpendicular combination of sending and receiving panels

Let us consider the interaction of a perpendicular combination of receiving panel r and sending panel s. Utilising the expressions developed in Appendix E, the numerator of Equation 5.1 can be written, for the steady case, as:

$$K_0r^2 = \frac{At^2 + Bt + C}{a_rt^2 + b_rt + c_r} \qquad \text{F.1}$$

where the coefficients A, B and C are defined in Equations E.19 to E.21 and the coefficients a_r, b_r and c_r are defined in Equations E.7 to E.9. Since the panels are perpendicular $\cos(\gamma_r - \gamma_s) = 0$, and Equation F.1 becomes:

$$K_0r^2 = \frac{a_3K_2^{(S)}(a_2t + a_1)}{a_rt^2 + b_rt + c_r} \qquad \text{F.2}$$

where the coefficients a_1, a_2 and a_3 have been defined in Equations E.22 to E.24.

If we assume that $K_2^{(S)}$ is constant for the panel combination under consideration, then:

$$\frac{d(K_0r^2)}{dt} = \frac{-a_3K_2^{(S)}(a_ra_2t^2 + 2a_ra_1t + b_ra_1 - c_ra_2)}{(a_rt^2 + b_rt + c_r)^2} \qquad \text{F.3}$$

After setting the above expression to zero, the positions of the turning points may be estimated by solving the following equation:

$$a_ra_2t^2 + 2a_ra_1t + b_ra_1 - c_ra_2 = 0 \qquad \text{F.4}$$

for the values of t.

APPENDIX G

Considerations in the selection of panel distributions

In the doublet lattice method the surface is divided into a number of panels. A number of rules and considerations apply to the choice of panel distribution for a given configuration; these are as follows:

1. The panels are trapezial in shape and the sides of panels must be aligned streamwise. Panels are arranged in strips parallel to the free-stream. The aspect ratio of the panels should not be large. For the unsteady case, an aspect ratio of order unity or less is preferred [Ref. 7].

2. Surface intersections, surface edges, control surface boundaries, fold lines and other discontinuities should lie on panel boundaries.

3. For wing-tail type configurations the strip boundaries on the tail must be aligned with those on the wing.

4. The analysis assumes that the pressure is constant over each panel. Thus the results will be more accurate if the panels are smaller where the pressure distribution varies more rapidly. Consequently the panels should be concentrated near the wing tips, the leading and trailing edges of the surface and near control surface edges. This also applies to all regions where the normalwash boundary conditions are discontinuous.

5. Where surfaces intersect, the panels should be arranged such that the sides of panels situated along the line of intersection do not overlap. This means that the spanwise lines must coincide as shown in Figure 17.

APPENDIX H

Input data for program AIRFORTP

Program AIRFORTP calculates the pressure distribution and generalised airforces for general lifting surface configurations oscillating in subsonic flow. The data file, AIRFOR . DAT, for this program has the following form :

```
GNU, AM, RL
IPLOT, IPRNTP
NONODE
I, XN(I), YN(I), ZN(I)
.
.
.
NGRPS
GROUPTITLE
J, J1NODE(J), J2NODE(J),J3NODE(J), J4NODE(J)
IREF(J, 1), IREF (J, 2), IREF (J, 3), IREF (J, 4)
NC(J), NS(J), NCEVEN, NSEVEN, ITCORD
(TCORD1 (J, K), K = 1, NC(J)+1)
(TCORD2 (J, K), K = 1, NC(J)+1)
(TSORDS (J, K), K = 1, NS(J)+1)
.
.
.
NGRPSA
(IGRPSA (K), K = 1, NGRPSA)
NMODEA
(IMODEA (K), K = 1, NMODEA)
```

where

GNU	frequency parameter, $\frac{\omega l}{U}$.
AM	Mach number. $AM < 1{\cdot}0$.
RL	reference length, l.
IPLOT	Flag for initiating preparation of data file for use in PIGS graphics package. IPLOT = 0 : no data preparation ; IPLOT = 1 : PAFEC data file, BOX . DAT, is created and program AIRFORTP stops execution.
IPRNT	Flag for choosing format of print out of the calculated pressure distributions.

IPRNT = 0: no pressures printed;
IPRNT = 1: pressures for each mode printed in column fashion;
IPRNT = 2: pressures for each mode printed in matrix array form for each group of panels.

NONODE — number of nodes to be defined. Nodes need not be numbered sequentially. $1 \leqslant$ NONODE $\leqslant 100$.

I — node identification number. $1 \leqslant I \leqslant 100$.

XN(I) — X coordinate of node I.
YN(I) — Y coordinate of node I.
ZN(I) — Z coordinate of node I.

NGRPS — number of groups (of panels) to be defined. Groups need not be numbered sequentially. $1 \leqslant$ NGRPS $\leqslant 50$.

GROUPTITLE — title to describe the group whose input data follows. Up to 70 characters are allowed. e.g. PORT WINGLET.

J — group identification number. $1 \leqslant J \leqslant$ NGRPS. Groups need not be numbered sequentially.

J1NODE(J)
J2NODE(J)
J3NODE(J)
J4NODE(J) — Node numbers defining the leading and trailing edges of group J. The sequence 1, 2, 3, 4 follows the group node numbering convention (defined in Section 8.1 and Fig. 8).

IREF (J, 1)
IREF (J, 2)
IREF (J, 3)
IREF (J, 4) — numbers defining the senses of positive pressures on the source group and any images that have been created. They may take the values 0, −1, +1 except for the source group IREF (J, 1), which must be non-zero. See Section 8.3 for a detailed description.

NC(J) — number of chordwise panels on group J.
NS(J) — number of spanwise panels on group J.

NCEVEN — flag for choosing whether or not panels down the chord of group J are to be evenly spaced.
NCEVEN 0: panels not evenly spaced.
NCEVEN 1: panels are evenly spaced.

NSEVEN — flag for choosing whether or not spanwise columns of panels on group J are to be evenly spaced.
NSEVEN 0: columns not evenly spaced.
NSEVEN 1: columns are evenly spaced.

ITCORD — flag for choosing whether or not the ordinates of chordwise edges of panels for the side containing nodes J2NODE(J) and J4NODE(J), TCORD2(J,K), are to be provided as input data. This feature allows panels of constant chord to be located on a tapered lifting surface. If ITCORD 0 then the line of data containing the ordinates TCORD2(J,K) is omitted and the program defaults to TCORD2(J,K) TCORD1(J,K). If ITCORD 1 then the line of data containing TCORD2(J,K) must be included.

TCORD1(J,K) ordinates of the chordwise edges of panels on group J, non-dimensionalised with respect to the local chord, for the side containing nodes J1NODE(J) and J3NODE(J). TCORD1(J,1) = 0·0 at the leading edge of the group and TCORD1(J,NC(J)+1) = 1·0 at the trailing edge. This line of input data is omitted if NCEVEN=1.

TCORD2(J,K) ordinates of the chordwise edges of panels on group J, non-dimensionalised with respect to the local chord, for the side containing nodes J2NODE(J) and J4NODE(J). TCORD2(J,1) = 0·0 at the leading edge of the group and TCORD2(J,NC(J)+1) = 1·0 at the trailing edge. This line of input data is omitted if NCEVEN = 1 or ITCORD = 0.

TSORDS(J,K) ordinates of the spanwise edges of columns of panels on group J, nondimensionalised with respect to the span of group J. TSORDS(J,1) = 0·0 at the streamwise side containing node J1NODE(J), and TSORDS(J,NS(J)+1) = 1·0 at the streamwise side containing node J2NODE(J). This line of input data is omitted if NSEVEN = 1.

NGRPSA number of source groups, together with any defined images, to be included in the analysis. The groups for analysis are chosen from the set of groups that have been defined earlier in the data file. $1 \leqslant$ NGRPSA $\leqslant 50$.

IGRPSA(K) list of NGRPSA group numbers identifying the subset of groups to be included in the analysis from the set of groups defined previously. The numbers may be in any sequence.

NMODEA number of modes which are to be used in the analysis. $1 \leqslant$ NMODEA $\leqslant 20$.

IMODEA(K) list of NMODEA mode numbers that identifies the subset of modes for which the analysis is to be carried out. The numbers in the list refer to the mode numbers defined in SUBROUTINE MODES. The numbers may be in any order.

The data file is primarily concerned with information related to the geometry of the configuration being analysed. In order to obtain pressures and generalised forces it is necessary to supply a SUBROUTINE MODES which defines the modal data to be used by program AIRFORCE. The modal data consists of nondimensional displacements and slopes at the normalwash collocation points and, in order to calculate the generalised forces, the nondimensional displacements at the lift points must also be defined. This information must be stored in a labelled COMMON MODATA as follows:

```
PARAMETER (NP = 260, NM = 20)
COMMON /MODATA/ NOMODE, DZL(NP,NM), DZD(NP,NM), DAD(NP,NM)
```

The variables associated with the above COMMON block are defined as follows:

NP maximum number of panels which can be used. This is currently set to NP = 260.

NM maximum number of modes for which pressures can be calculated. This is currently set to NM = 20.

NOMODE total number of modes that are defined where NOMODE $\leqslant$ NM. The input list of modes to be used in the analysis defines which modes are to be used.

DZL(N,M) — nondimensional displacement at the lift point on panel N in mode M.

DZD(N,M) — nondimensional displacement at the normalwash collocation point on panel N in mode M.

DAD(N,M) — slope at the normalwash collocation point on panel N in mode M.

The nondimensional displacements are normalised with respect to the reference length. Panel N corresponds to the panel in the I'th row and J'th column of the K'th group. N is given by:

$$N = INDEXS(K)+(J-1)*NC(K)+I \qquad \begin{matrix} 1 \leqslant J \leqslant NS(K) \\ 1 \leqslant J \leqslant NC(K) \end{matrix} \qquad \text{H.1}$$

and the vectors INDEXS, NC and NS are described in the following section.

In order to facilitate the preparation of the modal data, the specifications of a number of labelled COMMON blocks are given below. These COMMON blocks contain data related to the geometry of the configuration, as well as information associated with the organisation of this data, and are given below (note that NP was defined previously):

```
PARAMETER (NE = 50)

COMMON/AERPAR/GNU, AM, RL, AM2, BETA2, BETA, RL2
COMMON/XYZLFT/XL(NP,4), YL(NP,4), ZL(NP,4)
COMMON/XYZDSH/XD(NP,4), YD(NP,4), ZD(NP,4)
COMMON/ INDEX /INDEXS(NE), INDEXA(NE)
COMMON/ELDATA/NOELEM, NC(NE), NS(NE), IREF(NE,4), IELUSE(NE)
COMMON/DIHEDL/DIHEDL(NE,4)
```

The definitions of the variables are:

NE — maximum number of groups which can be defined. This is currently set to NE = 50.

GNU — frequency parameter

AM — Mach number

RL — reference length

AM2 — AM * AM

BETA2 — 1.0 - AM * AM

BETA — SQRT (BETA)

RL2 — RL * RL

XL(N,IR), YL(N,IR), ZL(N,IR) — dimensional (X, Y, Z) coordinates of the lift point on the N'th panel in the IR'th reflection state. IR = 1 refers to the source group (see Section 8.3).

XD(N,IR), YD(N,IR), ZD(N,IR) — dimensional (X, Y, Z) coordinates of the normalwash collocation point on the N'th panel in the IR'th reflection state.

INDEXS(K) — pointer indexing the position of the first panel associated with the K'th group. This pointer refers to all source groups.

INDEXA(K)	pointer indexing the position of the first panel associated with the K'th group used in the analysis.
NOELEM	number of groups (elements) defined in the data file.
NC(K)	number of chordwise panels for the K'th group.
NS(K)	number of spanwise panels for the K'th group.
IREF(K,IR)	number defining the sense of positive pressure on the K'th source group (IR = 1) and any image groups (IR = 2, 3 or 4). See the definition of IREF used in relation to the input data file.
IELUSE(K)	this variable indicates whether a particular group (element) number has been used. If IELUSE(K) = 0 then the K'th group (element) has not been defined. If IELUSE(K) = 1 then the K'th group has been defined.
DIHEDL(K,IR)	this is the dihedral angle (in radians) of the K'th group. IR = 1 refers to the source group and IR = 2, 3 and 4 refer to any image groups that were created.

Let us consider the N'th panel oscillating in mode M. The coordinates of the normalwash collocation point may be given as (x_N, y_N, z_N), and by applying Equation 6.1 the displacement normal to the surface at the collocation point may be expressed in the following form :

$$Z_M(x_N, y_N, z_N, t) = -l f_M(x_N, y_N, z_N) e^{i\omega t} \qquad \text{H.2}$$

The coordinates of the normalwash collocation point on the N'th source panel are given by the following equation :

$$(x_N, y_N, z_N) = (XD(N,1),\ YD(N,1),\ ZD(N,1)) \qquad \text{H.3}$$

Using Equation 6.3 the nondimensional normalwash may be expressed as

$$\frac{w_M(x_N, y_N, z_N)}{U} = \frac{\partial}{\partial(x/l)}\left(f_M(x_N, y_N, z_N) \right) + ik f_M(x_N, y_N, z_N) \qquad \text{H.4}$$

$$\text{DAD(N,M)} + ik \cdot \text{DZD(N,M)} \qquad \text{H.5}$$

In order to obtain the generalised forces it is necessary to calculate the nondimensional displacement at the mid-span quarter-chord point of the N'th source panel, $(\hat{x}_N, \hat{y}_N, \hat{z}_N)$, in the M'th mode. The nondimensional displacement may be determined from the following equation :

$$f_M(\hat{x}_M, \hat{y}_M, \hat{z}_M) = f_M(XL(N,1),\ YL(N,1),\ ZL(N,1)) \qquad \text{H.6}$$

$$DZL(N,M) \qquad \text{H.7}$$

Although it is customary to define DZL in the manner depicted above, this convention need not be followed if forces other than generalised forces are required.

A sign convention exists for the specification of the modal displacements and slopes used in the calculation of pressures and generalised forces. The displacements perpendicular to the surface, DZD and DZL, are taken to be positive when they are in the same direction on a group as the direction of positive pressure for that group. The slope at the normalwash collocation point, DAD, is positive if the displacement at that point, DZD, is increasing in the streamwise (x) direction. An example illustrating the application of the above convention is given in Appendix I.

APPENDIX I

Example of input preparation for the analysis of Stark's T-tail

As an illustrative example, the preparation of the input data file and SUBROUTINE MODES for Stark's T-tail will be described. The configuration is assumed to be oscillating with a frequency parameter of 0·6, based on a reference length of one unit, in an airstream of Mach number 0·8.

The data file for the panel distribution shown in Figure 17 is given in Table 13. A total of 7 nodes were used to define the configuration. The positions of the nodes can be deduced by using the node coordinates in conjunction with Figure 16. Two groups were defined, with group 1 corresponding to the starboard half of the stabiliser and group 2 corresponding to the fin.

Due to symmetry, only the starboard half of the stabiliser is modelled. Nodes 1 and 2 define the leading edge and nodes 3 and 4 define the trailing edge of the stabiliser. IREF(1,1) = 1 indicates that the direction of positive pressure on the source group is in the negative z-direction. This agrees with the topology of the group (see Section 8.2). The effect of the port half of the stabiliser is included by setting IREF(1,2) = 1. This creates an image of the source group by reflection in the x–z plane.

The positive sense of pressure on the image is in the positive z-direction, which once again corresponds with the topology of the group. The combination of positive pressures on the port and starboard halves of the stabiliser corresponds to antisymmetric motion of the stabiliser.

The stabiliser is divided into 11 panels chordwise and 10 panels spanwise, with the chordwise panel distribution being the same on both sides of the half stabiliser. The chordwise and spanwise ordinates of the panel sides are listed in lines 16 and 17 of the data file.

The leading edge of the fin is defined by nodes 2 and 5 and the trailing edge by nodes 6 and 7. Since IREF(2,1) = −1, the sense of positive pressure on the fin is in the negative y-direction which is opposite to that defined by the topology of this source group. Note that no image surfaces are created. The fin is divided into 9 panels chordwise and 10 panels spanwise, and the nondimensional ordinates of the panel sides are listed in lines 22 and 23 of the data file.

For this analysis, both the stabiliser and fin are included, which is indicated in lines 24 and 25. Three modes are to be used in the calculation of pressures and generalised forces. The numbers 1, 2 and 3 in the last line refer to the modes defined in SUBROUTINE MODES.

Since IPLOT = 0 (see line 2) a PAFEC data file for use in PIGS will not be created. By setting IPRNTP = 1 the print out of pressures associated with the three modes will be presented in a columnar format.

A SUBROUTINE MODES is required to generate the modal data and a detailed description of the format of this subroutine is given in Appendix H. A listing of the FORTRAN source code for the subroutine used to calculate modal displacements for Stark's T-tail is presented in Table 14.

As described in Section 9.2, the T-tail is assumed to be oscillating in three rigid body modes. These are yawing about a vertical axis through the centre of the root chord of the fin (positive nose right), sidesway (positive left) and rolling about the fin-stabiliser intersection (positive right stabiliser down). These modes are expressed analytically in Equations 9.5 to 9.10, and when they are used in Equations H.4 to H.7 the following equations are obtained for the stabiliser:

DZD(N,1) DAD(N,1) DZL(N,1) 0·0 I.1

DZD(N,2) DAD(N,2) DZL(N,2) 0·0 I.2

DZD(N,3) YD(N,1) I.3

$$DAD(N,3) = 0{\cdot}0 \tag{I.4}$$

$$DZL(N,3) = YL(N,1) \tag{I.5}$$

where

$$N = INDEXS(K)+(J-1)*NC(K)+I \tag{I.6}$$

$$1 \leqslant I \leqslant NC(K) \tag{I.7}$$

$$1 \leqslant J \leqslant NS(K) \tag{I.8}$$

and K = 1 for the stabiliser group. The modal data for the fin is as follows:

$$DZD(N,1) = 3{\cdot}0 * (XD(N,1)+0{\cdot}15577) \tag{I.9}$$

$$DAD(N,1) = 3{\cdot}0 \tag{I.10}$$

$$DZL(N,1) = 3{\cdot}0 * (XL(N,1)+0{\cdot}15577) \tag{I.11}$$

$$DZD(N,2) = 1{\cdot}0 \tag{I.12}$$

$$DAD(N,2) = 0{\cdot}0 \tag{I.13}$$

$$DZL(N,2) = 1{\cdot}0 \tag{I.14}$$

$$DZD(N,3) = -ZD(N,1) \tag{I.15}$$

$$DAD(N,3) = 0{\cdot}0 \tag{I.16}$$

$$DZL(N,3) = -ZL(N,1) \tag{I.17}$$

where N is obtained from Equations I.6 to I.8 by substituting K = 2 for the fin group.

Note that the displacements DZL and DZD are positive in the same direction as the sense of positive pressure that is defined for the panels in a given group. The slope DAD is positive if the displacement is increasing in the streamwise x-direction.

Figure 20 illustrates the mode shapes for the three modes used for Stark's T-tail. The + sign indicates that the displacement is in the same direction as the sense of positive pressure acting on the group, and the − sign indicates that the displacement is in the direction opposite to that of the positive pressure. Hence, where the + sign applies the displacements are positive quantities and where the − sign applies the displacements are negative quantities. It is seen that when the analytic expressions for the mode shapes are combined with the topology of the groups (as defined in the input data file) then the displacements depicted in Figure 20 are obtained.

TABLE 1

Values of Generalised Airforces, Q_{pq}, for the AGARD Wing–Tailplane Configuration (for h = 0) as Obtained by Different Workers

$h = 0$ $M = 0{\cdot}8$	Q_{pq}	Davies	Albano Perkinson Rodden	Albano Rodden	Geising Kalman Rodden	Farrell	Present Method
$k = 0$	$\lvert Q_{11} \rvert$	0·4403	0·4425	0·4554	0·4401	0·4377	0·4557
	$\angle Q_{11}$	359·9	359·9	359·9	359·9	360·0	360·0
	$\lvert Q_{12} \rvert$	0·6202	0·6121	0·6655	0·6557	0·6457	0·6652
	$\angle Q_{12}$	180·0	180·0	180·0	180·0	180·0	180·0
	$\lvert Q_{21} \rvert$	0·1046	0·1054	0·1107	0·1044	0·1049	0·1083
	$\angle Q_{21}$	180·3	180·3	180·3	180·3	180·0	180·0
	$\lvert Q_{22} \rvert$	0·1759	0·1954	0·2237	0·2126	0·2184	0·2261
	$\angle Q_{22}$	180·2	180·2	180·2	180·2	180·0	180·0
$k = 1{\cdot}5$	$\lvert Q_{11} \rvert$	1·5865	1·6022	1·5496	1·5688	1·4212	1·5713
	$\angle Q_{11}$	314·2	314·4	311·2	310·7	312·3	310·8
	$\lvert Q_{12} \rvert$	0·9180	0·8910	0·9081	0·9495	0·8752	0·9482
	$\angle Q_{12}$	265·5	266·3	267·2	265·4	265·0	265·8
	$\lvert Q_{21} \rvert$	1·0043	1·0099	1·0550	1·0511	0·9507	1·0653
	$\angle Q_{21}$	291·7	291·4	287·2	288·5	289·9	289·0
	$\lvert Q_{22} \rvert$	1·2845	1·2386	1·2144	1·2719	1·1448	1·2745
	$\angle Q_{22}$	294·7	294·3	293·7	292·9	294·1	293·2

TABLE 2

Values of Generalised Airforces, Q_{pq}, for the AGARD Wing–Tailplane Configurations as Obtained by Different Workers

$h = 0{\cdot}6$ $M = 0{\cdot}8$	Q_{pq}	Davies	Albano Perkinson Rodden	Farrell	Present Method
$k = 0$	$\lvert Q_{11} \rvert$	0·1470	0·1490	0·1374	0·1432
	$\angle Q_{11}$	359·8	359·8	360·0	360·0
	$\lvert Q_{12} \rvert$	0·6402	0·6312	0·6661	0·6868
	$\angle Q_{12}$	180·1	180·1	180·0	180·0
	$\lvert Q_{21} \rvert$	0·2404	0·2405	0·2527	0·2669
	$\angle Q_{21}$	180·1	180·1	180·0	180·0
	$\lvert Q_{22} \rvert$	0·1619	0·1817	0·1958	0·2117
	$\angle Q_{22}$	180·3	180·2	180·0	180·0
$k = 1{\cdot}5$	$\lvert Q_{11} \rvert$	1·1009	1·1200	0·9780	1·0837
	$\angle Q_{11}$	301·3	301·3	299·9	298·3
	$\lvert Q_{12} \rvert$	1·1342	1·1128	1·0735	1·1583
	$\angle Q_{12}$	251·7	251·9	249·5	250·0
	$\lvert Q_{21} \rvert$	0·9072	0·9122	0·8259	0·9239
	$\angle Q_{21}$	278·0	277·7	276·9	275·8
	$\lvert Q_{22} \rvert$	1·3867	1·3397	1·2082	1·3541
	$\angle Q_{22}$	289·2	288·6	287·2	286·4

TABLE 3

Generalised Airforces for the AGARD Wing–Tailplane Configuration (with h = 0·6, M = 0·8) for a Range of Frequency Parameters

$h=0{\cdot}6$ $M=0{\cdot}8$	$\lvert Q_{11}\rvert$ $\angle Q_{11}$		$\lvert Q_{12}\rvert$ $\angle Q_{12}$		$\lvert Q_{21}\rvert$ $\angle Q_{21}$		$\lvert Q_{22}\rvert$ $\angle Q_{22}$	
k	Davies	Present Method	Davies	Present Method	Davies	Present Method	Davies	Present Method
0	0·1470 359·8	0·1432 360·0	0·6402 180·1	0·6868 180·0	0·2404 180·1	0·2669 180·0	0·1619 180·3	0·2117 180·0
0·1	0·1588 339·8	0·1563 338·1	0·6418 185·5	0·6885 185·4	0·244 192·5	0·2715 192·3	0·1763 205·4	0·2234 200·7
0·2	0·1899 324·6	0·1907 322·1	0·6466 191·1	0·6933 190·7	0·2571 204·4	0·2850 203·9	0·2140 225·1	0·2555 218·1
0·4	0·2840 308·8	0·2916 306·0	0·6665 202·0	0·7123 201·3	0·3036 224·8	0·3346 223·8	0·3274 248·7	0·3589 242·0
0·6	0·4001 302·7	0·4114 300·0	0·7021 212·8	0·7462 211·8	0·3726 240·4	0·4071 239·0	0·4670 262·1	0·4924 256·5
0·8	0·5301 300·6	0·5428 297·8	0·7560 223·0	0·7984 221·9	0·4595 252·3	0·4966 250·6	0·6265 271·1	0·6461 266·5
1·0	0·6737 300·2	0·6844 297·3	0·8310 232·5	0·8715 231·2	0·5632 261·7	0·6003 259·7	0·8079 278·0	0·8195 274·0
1·2	0·8320 300·5	0·8358 297·5	0·9308 241·1	0·9676 239·6	0·6847 269·2	0·7179 267·1	1·0156 283·4	1·0148 279·9
1·5	1·1009 301·3	1·0837 298·3	1·1342 251·7	1·1583 250·0	0·9072 278·0	0·9239 275·8	1·3867 289·2	1·3541 286·4

TABLE 4

Generalised Airforces for the AGARD Wing–Tail Configuration for Various Values of Vertical Separation, h, Between Wing and Tail

$k=1\cdot5$ $M=0\cdot8$	$\lvert Q_{11}\rvert$ $\angle Q_{11}$		$\lvert Q_{12}\rvert$ $\angle Q_{12}$		$\lvert Q_{21}\rvert$ $\angle Q_{21}$		$\lvert Q_{22}\rvert$ $\angle Q_{22}$	
h	Davies	Present Method	Davies	Present Method	Davies	Present Method	Davies	Present Method
0	1·5865 314·2	1·5713 310·8	0·9180 265·5	0·9482 265·8	1·0043 291·7	1·0653 289·0	1·2845 294·7	1·2745 293·2
0·01	1·5519 313·3	1·5514 310·7	0·9332 264·0	0·9520 264·9	0·9973 290·4	1·0574 288·7	1·2890 294·0	1·2734 292·8
0·04	1·4773 311·4	1·4777 309·3	0·9640 261·2	0·9789 261·7	0·9843 287·7	1·0347 286·6	1·2992 292·6	1·2782 291·3
0·1	1·3730 308·7	1·3605 306·1	1·0040 258·0	1·0303 257·5	0·9662 284·3	1·0042 282·8	1·3151 291·3	1·2946 289·2
0·2	1·2624 305·9	1·2461 303·0	1·0479 255·2	1·0779 254·1	0·9428 281·4	0·9724 279·5	1·3376 290·4	1·3138 287·8
0·3	1·1948 304·0	1·1787 301·2	1·0790 253·7	1·1072 252·3	0·9271 279·8	0·9520 277·8	1·3559 290·0	1·3270 287·2
0·4	1·1511 302·8	1·1349 299·9	1·1024 265·8	1·1284 251·2	0·9174 279·0	0·9383 276·8	1·3695 289·7	1·3376 286·9
0·5	1·1216 301·9	1·1048 299·0	1·1204 252·2	1·1450 250·5	0·9113 278·4	0·9295 276·2	1·3795 289·5	1·3468 286·6
0·6	1·1009 301·3	1·0837 298·3	1·1342 251·7	1·1583 250·0	0·9072 278·0	0·9239 275·8	1·3867 289·2	1·3541 286·4

TABLE 5

Generalised Airforces for Stark's T-tail for Zero Frequency and Two Mach Numbers as Obtained by Different Workers

	$k = 0$ $M = 0$			$k = 0$ $M = 0{\cdot}8$		
Q_{pq}	Stark	Kalman Rodden Geising	Present Method	Stark	Kalman Rodden Geising	Present Method
Q_{11}	−0·6220	−0·6095	−0·5428	−0·8137	−0·7804	−0·7189
Q_{21}	−3·2503	−3·3647	−3·4020	−3·7366	−3·8768	−3·8924
Q_{31}	−0·7813	−0·7965	−0·8229	−0·7858	−0·7985	−0·8257

TABLE 6

Generalised Airforces for Stark's T-tail as Obtained by Different Workers

	$k = 0{\cdot}6$ $M = 0{\cdot}8$						$k = 0{\cdot}9$ $M = 0{\cdot}8$		
Q_{pq}	Stark	Davies	Zwaan	Kalman Rodden Geising	Farrell	Present Method	Stark	Farrell	Present Method
$\lvert Q_{11} \rvert$	3·0826	3·2421	3·2873	3·3527	2·7470	3·0965	4·8800	4·1775	4·8056
$\angle Q_{11}$	258·8	260·6	259·8	261·0	260·6	260·5	264·9	266·2	265·5
$\lvert Q_{12} \rvert$	0·3202	0·3399	0·3475	0·3431	0·2799	0·3214	0·7020	0·6016	0·7042
$\angle Q_{12}$	323·9	328·5	327·4	329·4	328·1	328·1	330·6	333·7	332·7
$\lvert Q_{13} \rvert$	0·1695	0·1859	0·1865	0·1830	0·1680	0·1828	0·3214	0·2971	0·3358
$\angle Q_{13}$	62·4	61·5	60·8	61·9	61·6	60·9	52·0	50·4	49·7
$\lvert Q_{21} \rvert$	4·4628	4·5670	4·5650	4·6612	4·4291	4·6085	5·3736	5·1126	5·4472
$\angle Q_{21}$	210·7	211·1	210·9	212·3	211·0	211·0	220·8	220·1	221·2
$\lvert Q_{22} \rvert$	0·7758	0·7930	0·7936	0·8134	0·7815	0·8072	1·2419	1·2185	1·2822
$\angle Q_{22}$	281·2	282·1	281·9	283·3	282·3	282·2	286·5	288·3	287·6
$\lvert Q_{23} \rvert$	0·2103	0·2191	0·2183	0·2269	0·2282	0·2330	0·3692	0·3882	0·4055
$\angle Q_{23}$	298·2	299·0	298·9	298·3	296·6	297·8	310·2	307·6	309·0
$\lvert Q_{31} \rvert$	1·0772	1·1154	1·1006	1·1383	1·1483	1·1686	1·3760	1·4446	1·4903
$\angle Q_{31}$	222·7	224·7	224·6	224·9	225·3	224·9	232·1	236·6	235·3
$\lvert Q_{32} \rvert$	0·1810	0·1897	0·1874	0·1948	0·2000	0·2022	0·3214	0·3484	0·3557
$\angle Q_{32}$	297·7	299·8	299·7	299·8	300·1	299·7	305·8	308·5	307·6
$\lvert Q_{33} \rvert$	0·3319	0·3349	0·3349	0·3523	0·3590	0·3617	0·5484	0·5794	0·5910
$\angle Q_{33}$	289·8	289·6	289·6	289·4	288·8	289·4	298·1	296·8	297·5

TABLE 7

Comparison of Results for Stark's T-tail Obtained with Different Panel Distributions. The Top Table Indicates the Panel Distributions Used

		Surface	No. Panels Chordwise	No. Panels Spanwise
Present Method	Case 1	Fin	9	10
		Stabiliser	11	10
	Case 2	Fin	4	12
		Stabiliser	5	12
Farrell		Fin	4	12
		Stabiliser	4	12

	$k = 0{\cdot}6$ $\quad M = 0{\cdot}8$		
Q_{pq}	Present Method		Farrell
	Case 1	Case 2	
$\lvert Q_{11} \rvert$	3·0965	2·8362	2·7470
$\angle Q_{11}$	260·5	260·3	260·6
$\lvert Q_{12} \rvert$	0·3214	0·2908	0·2799
Q_{12}	328·1	327·5	328·1
$\lvert Q_{13} \rvert$	0·1828	0·1670	0·1680
$\angle Q_{13}$	60·9	62·6	61·6
$\lvert Q_{22} \rvert$	4·6085	4·5025	4·4291
$\angle Q_{22}$	211·0	211·3	211·0
$\lvert Q_{22} \rvert$	0·8072	0·7937	0·7815
$\angle Q_{22}$	282·2	282·5	282·3
$\lvert Q_{23} \rvert$	0·2330	0·2283	0·2282
$\angle Q_{23}$	297·8	296·9	296·6
$\lvert Q_{31} \rvert$	1·1686	1·1467	1·1483
$\angle Q_{31}$	224·9	225·4	225·3
$\lvert Q_{32} \rvert$	0·2022	0·2000	0·2000
$\angle Q_{32}$	299·7	300·2	300·1
$\lvert Q_{33} \rvert$	0·3617	0·3607	0·3590
$\angle Q_{33}$	289·4	289·0	288·8

TABLE 8

Generalised Airforces for the ONERA Horizontal Wing and Tail Configuration for H 1/8 and λ 2

$H=1/8$ $\lambda=2$	$M=0\cdot30$ $k=0\cdot3856$		$M=0\cdot45$ $k=0\cdot2436$		$M=0\cdot65$ $k=0\cdot1513$		$M=0\cdot80$ $k=0\cdot1112$	
Q_{pq}	Davies	Present Method	Davies	Present Method	Davies	Present Method	Davies	Present Method
$\lvert Q_{33}\rvert$	14·209	14·068	14·786	14·850	16·248	16·396	18·346	18·620
$\angle Q_{33}$	349·9	354·8	353·2	355·6	354·0	355·7	353·4	354·9
$\lvert Q_{34}\rvert$	0·214	0·244	0·234	0·260	0·220	0·241	0·181	0·196
$\angle Q_{34}$	311·7	307·6	311·3	309·6	301·2	300·9	273·9	273·9
$\lvert Q_{43}\rvert$	8·057	8·252	8·518	8·675	9·897	10·039	12·066	12·293
$\angle Q_{43}$	116·4	112·5	138·4	136·0	152·3	150·8	157·4	156·3
$\lvert Q_{44}\rvert$	14·130	14·041	14·743	14·804	16·198	16·342	18·301	18·572
$\angle Q_{44}$	351·5	355·1	353·4	355·8	354·2	355·9	353·6	355·1
Q_{11}	1·066	1·221	1·150	1·290	1·081	1·194	0·872	0·957
Q_{11}	147·7	143·5	144·9	143·0	135·8	135·3	114·7	114·5
Q_{23}	29·102	30·196	30·456	31·464	34·703	35·716	41·054	42·315
Q_{23}	296·3	292·0	318·7	316·1	333·3	331·6	339·2	337·9

TABLE 9

Generalised Airforces for the ONERA Horizontal Wing and Tailplane Configuration for H = 1/8 and λ = 1/2

$H=1/8$ $\lambda=1/2$	$M=0\cdot30$ $k=0\cdot3856$		$M=0\cdot45$ $k=0\cdot2436$		$M=0\cdot65$ $k=0\cdot1513$		$M=0\cdot80$ $k=0\cdot1112$	
Q_{pq}	Davies	Present Method	Davies	Present Method	Davies	Present Method	Davies	Present Method
$\lvert Q_{33}\rvert$	13·847	13·797	14·417	14·503	15·889	16·058	18·075	18·381
$\angle Q_{33}$	352·7	356·39	354·3	356·8	354·9	356·7	354·4	355·8
$\lvert Q_{34}\rvert$	0·900	0·893	0·928	0·929	0·857	0·852	0·702	0·693
$\angle Q_{34}$	324·2	321·89	326·4	325·2	318·3	320·6	305·1	302·7
$\lvert Q_{13}\rvert$	7·934	8·118	8·415	8·561	9·732	9·865	11·813	12·025
$\angle Q_{13}$	156·1	152·1	164·1	161·7	168·9	167·3	170·1	169·0
$\lvert Q_{44}\rvert$	13·279	13·163	13·794	13·812	15·200	15·298	17·345	17·562
$\angle Q_{44}$	353·8	357·7	355·1	357·8	355·6	357·4	355·1	356·7
$\lvert Q_{14}\rvert$	6·381	6·791	6·641	7·106	6·446	6·886	5·666	6·067
$\angle Q_{14}$	165·5	164·0	164·5	163·8	161·2	161·1	153·4	153·7
$\lvert Q_{23}\rvert$	28·082	29·073	29·469	30·370	33·518	34·429	39·664	40·805
$\angle Q_{23}$	334·9	330·7	343·7	341·1	349·3	347·6	351·4	350·1

TABLE 10

Coefficients in Laschka's Approximation to $u(1+u^2)^{-\frac{1}{2}}$ (from Ref. 7)

n	a_n
1	+ 0·24186198
2	− 2·7918027
3	+ 24·991079
4	− 111·59196
5	+271·43549
6	305·75288
7	41·183630
8	+545·98537
9	−644·78155
10	+328·72755
11	− 64·279511

TABLE 11

Abscissas p_i and Coefficients a_i, b_i and c_i (for i 1 to 3) Used in Integration Scheme when $r^2 > 0$

i	p_i	a_i	b_i	c_i
1	0·774596669	0·833333333	−0·645497224	0·0
2	0·0	1·666666667	0·0	1·0
3	0·774596669	0·833333333	0·645497224	0·0

TABLE 12

Abscissas and Weights, p_i and C_i, for "Finite Part" Integration

$$\int_{-1}^{+1} \frac{f(p)}{p^2}\,dp \approx \sum_{i=1}^{9} C_i f(p_i)$$

i	p_i	C_i
1	0·984807753	0·007642844
2	0·866025404	0·469841270
3	0·642787610	0·003167376
4	0·342020143	5·610810220
5	0·0	14·139682541
6	0·342020143	5·610810220
7	0·642787610	0·003167376
8	0·866025404	0·469841270
9	0·984807753	0·007642844

TABLE 13

Listing of data file used for the analysis of Stark's T-tail configuration

```
0·6  0·8  1·0
0 1
7
1       0·341    1·0       0·0
2       0·000    0·0       0·0
3       0·813    1·0       0·0
4       0·938    0·0       0·0
5       0·801    0·0       1·0
6       0·820    0·0       0·0
7       0·489    0·0      -1·0
2
STABILISER
1  1  2  3  4
1  1  0  0
11  10  0  0  0
0·0  ·05245  ·13113  ·21855  ·36716  ·50704  ·65565  ·74307  ·82175  ·87420  ·941  1·0
0·0  ·04  ·10  ·18  ·30  ·50  ·70  ·82  ·90  ·96  1·0
FIN
2  2  5  6  7
 -1  0  0  0
9  10  0  0  0
0·0  ·06  ·15  ·25  ·42  ·58  ·75  ·85  ·94  1·0
0·0  ·04  ·10  ·18  ·30  ·50  ·70  ·82  ·90  ·96  1·0
2
1  2
3
1  2  3
```

TABLE 14

Listing of FORTRAN source code for the subroutine used to generate the modal data for Stark's T-tail configuration

```
C
CCCCCCCCCCCCCCCCCCCCCCCCCCCCCCCCCCCCCCCCCCCCCCCCCCCCCCCCCCCCCCC
C
      SUBROUTINE MODES
C
C  THIS SUBROUTINE CALCULATES THE MODES FOR THE UNSTEADY
C  AERODYNAMICS PROGRAM.
C
C  THE MODES ARE FOR STARK'S T-TAIL.
C
C    MODE 1: YAW
C    MODE 2: SIDESLIP
C    MODE 3: ROLL
C
CCCCCCCCCCCCCCCCCCCCCCCCCCCCCCCCCCCCCCCCCCCCCCCCCCCCCCCCCCCCCCC
C
      PARAMETER (NP=260,NE=50,NM=20)
C
      COMMON/AERPAR/GNU,AM,RL
      COMMON/XYZLFT/XL(NP,4),YL(NP,4),ZL(NP,4)
      COMMON/XYZDSH/XD(NP,4),YD(NP,4),ZD(NP,4)
      COMMON/ELDATA/NOELEM,NC(NE),NS(NE),IREF(NE,4)
      COMMON/INDEX/INDEXS(NE),INDEXA(NE)
C
      COMMON/MODATA/NOMODE,DZL(NP,NM),DZD(NP,NM),DAD(NP,NM)
C
C  NUMBER OF MODES DEFINED
C
      NOMODE=3
C
C  MODES FOR STABILISER: GROUP 1
C
      DO 10 N=INDEXS(1)+1,INDEXS(1)+NC(1)*NS(1)
C
      DZD(N,1)=0·0
      DAD(N,1)=0·0
      DZL(N,1)=0·0
C
      DZD(N,2)=0·0
      DAD(N,2)=0·0
      DZL(N,2)=0·0
C
      DZD(N,3)=+YD(N,1)
      DAD(N,3)=0·0
      DZL(N,3)=-YL(N,1)
C
   10 CONTINUE
C
C  MODES FOR FIN: GROUP 2
C
```

TABLE 14 (Continued)

```
      DO 20 N=INDEXS(2)+1,INDEXS(2)+NC(2)*NS(2)
C
      DZD(N,1)=+3·0*(XD(N,1)+0·15577)
      DAD(N,1)=+3·0
      DZL(N,1) =+3·0*(XL(N,1)+0·15577)
C
      DZD(N,2)=+1·0
      DAD(N,2)=0·0
      DZL(N,2) =+1·0
C
      DZD(N,3)=-ZD(N,1)
      DAD(N,3)=0·0
      DZL(N,3) =-ZL(N,1)
C
   20 CONTINUE
C
      RETURN
      END
```

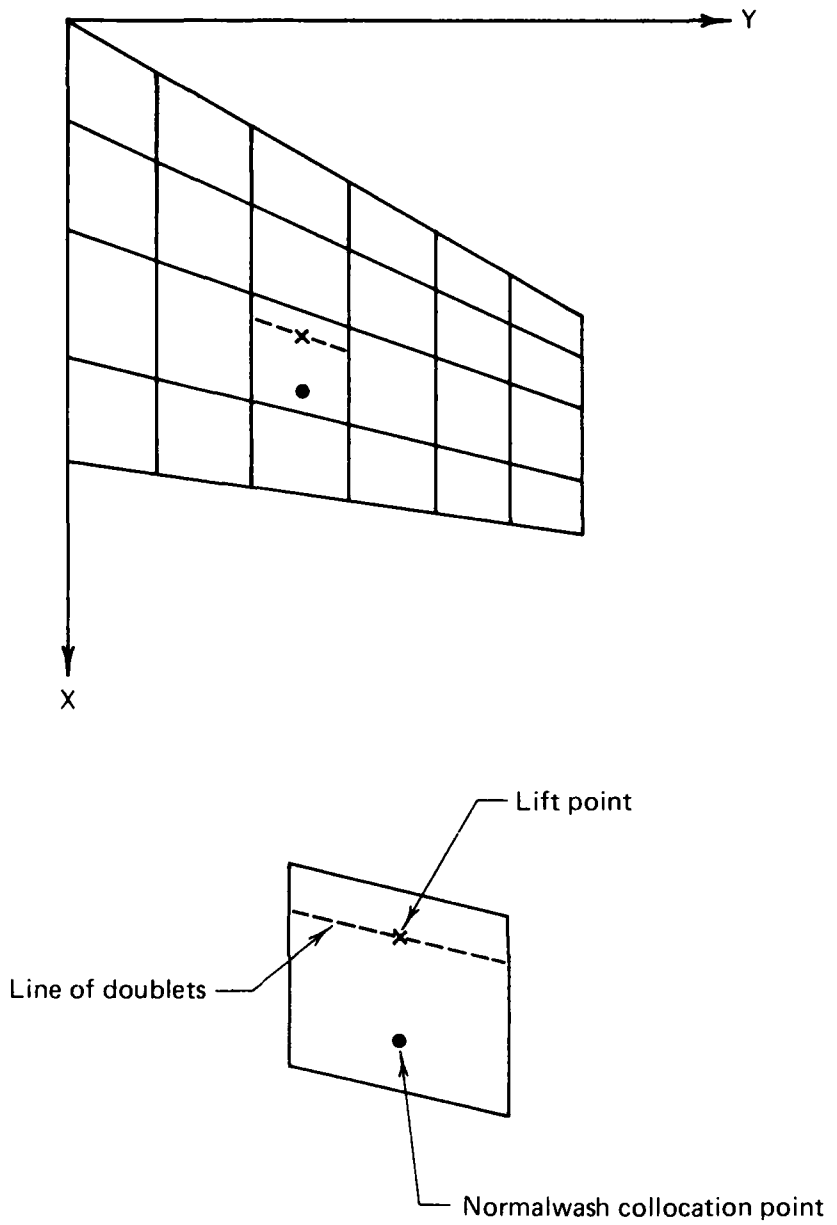

FIG. 1: EXAMPLE OF SURFACE REPRESENTATION BY PANELS AND THE FEATURES OF THE PANEL GEOMETRY.

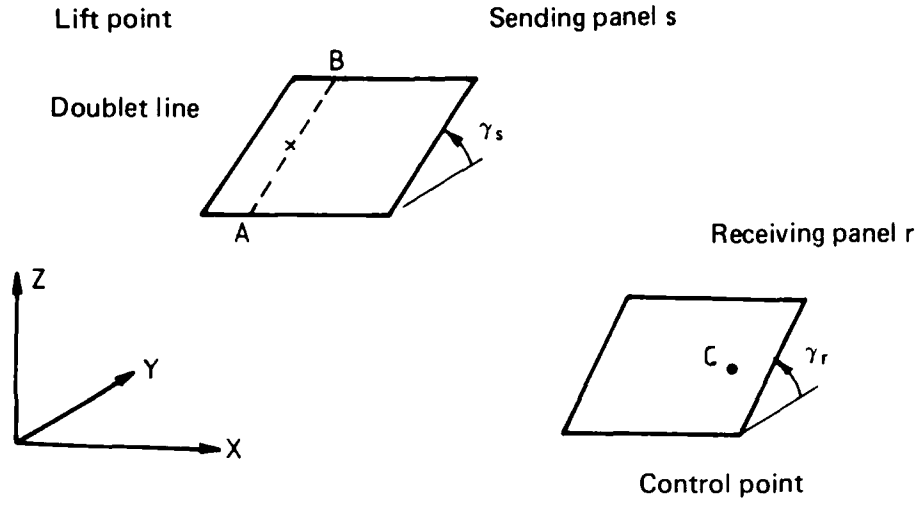

Point A: $(X, Y, Z) = (x_A, y_A, z_A)$

Point B: $(X, Y, Z) = (x_B, y_B, z_B)$

Point C: $(X, Y, Z) = (x, y, z)$

Panel dihedral angles : γ_s and γ_r

FIG. 2: DIAGRAM SHOWING A GENERAL COMBINATION OF A SENDING AND RECEIVING PANEL.

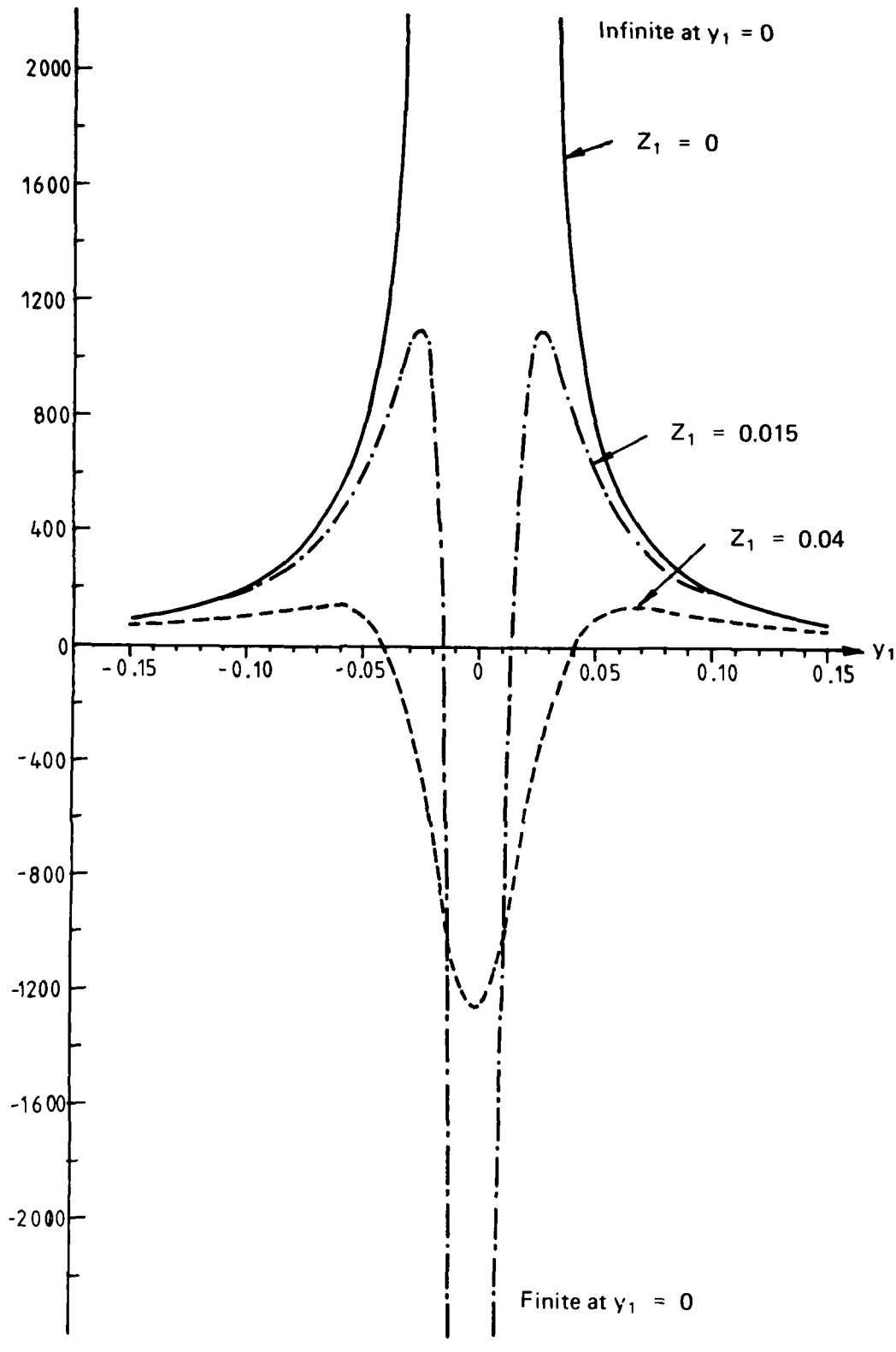

FIG. 3: COMPARISON OF NONPLANAR AND PLANAR KERNEL FUNCTIONS FOR k = 0 AND M = 0.6.

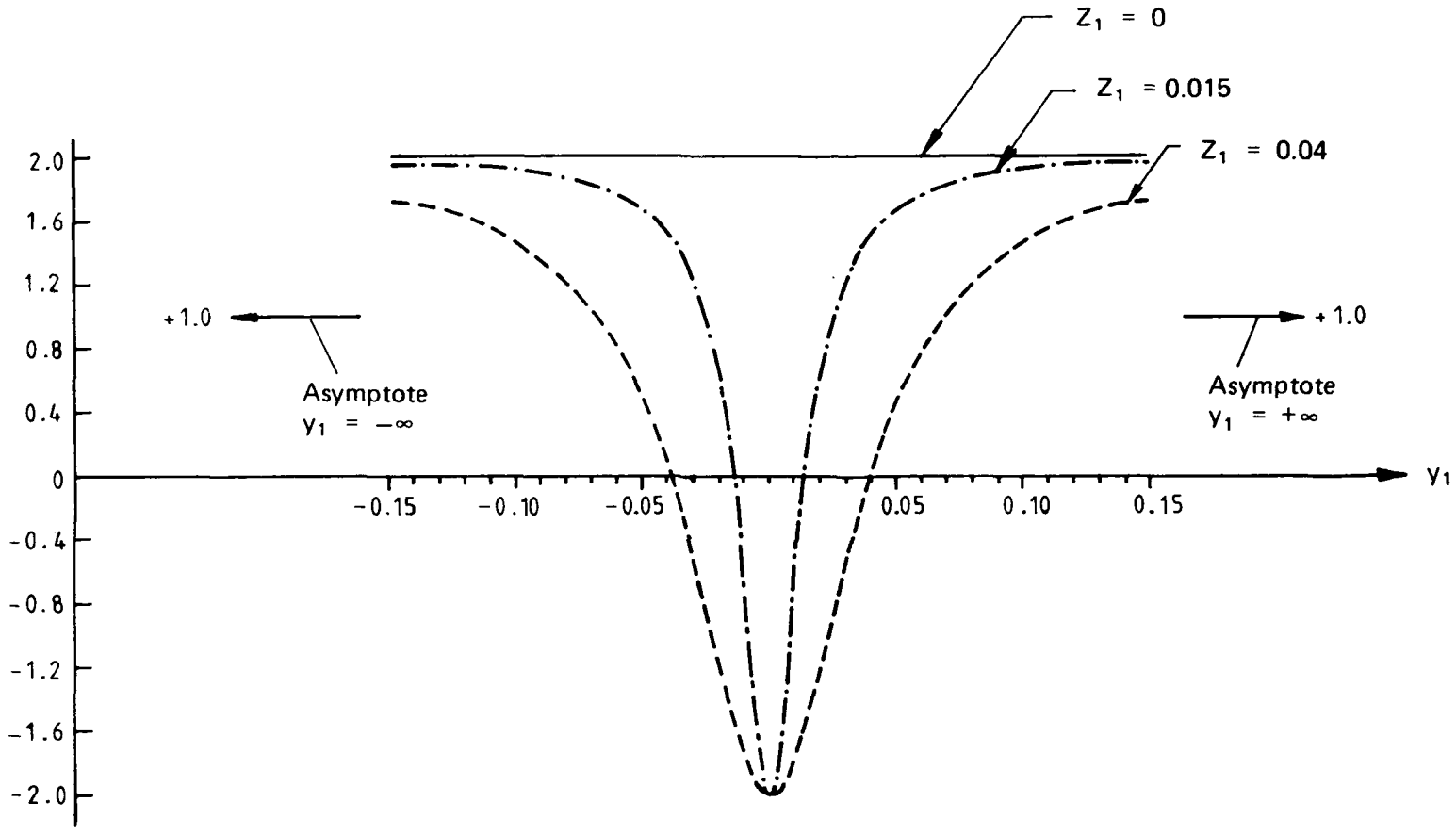

FIG. 4: COMPARISON OF NONPLANAR AND PLANAR PRODUCT OF THE STEADY KERNEL FUNCTION AND r^2, $K_o r^2$, *for* M = 0.6.

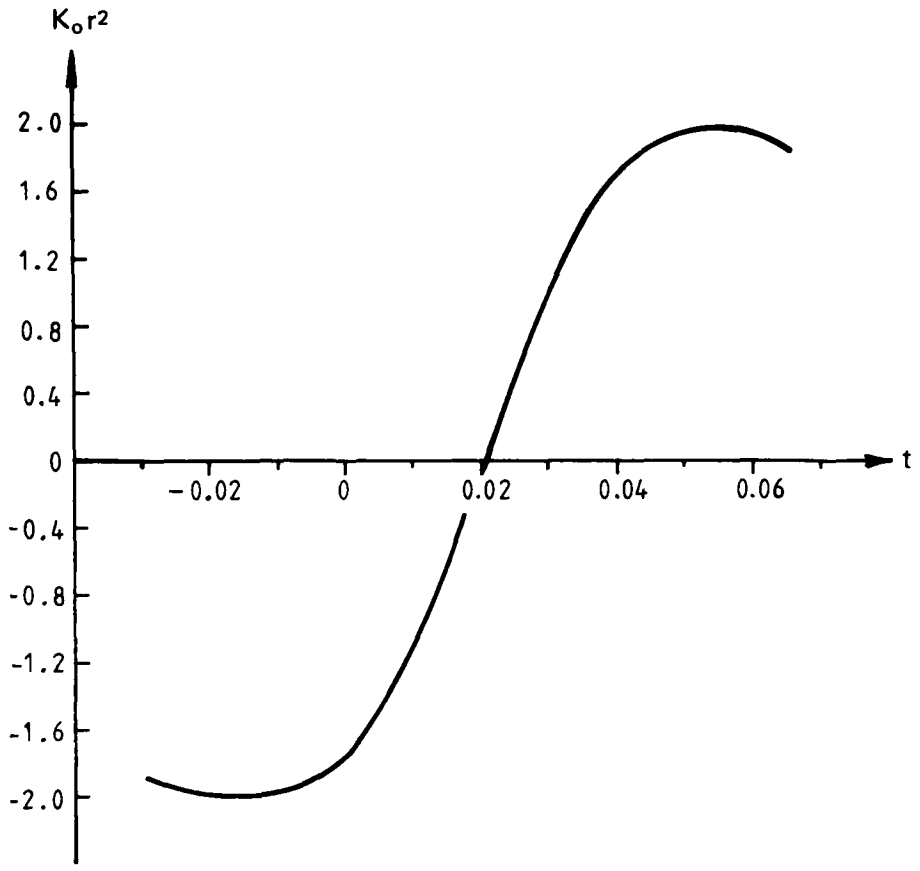

Parameters used in expression for $K_o r^2$:

$\gamma_i = 60^o \qquad \gamma_j = -30^o$

$M = 0.6$

$x_1 = 1.0$

$y_1 = \cos \gamma_j t$

$z_1 = \sin \gamma_j t + 0.04$

FIG. 5: VARIATION OF $K_o r^2$ FOR A SENDING AND RECEIVING PANEL COMBINATION WHERE THE PANELS ARE PERPENDICULAR TO EACH OTHER.

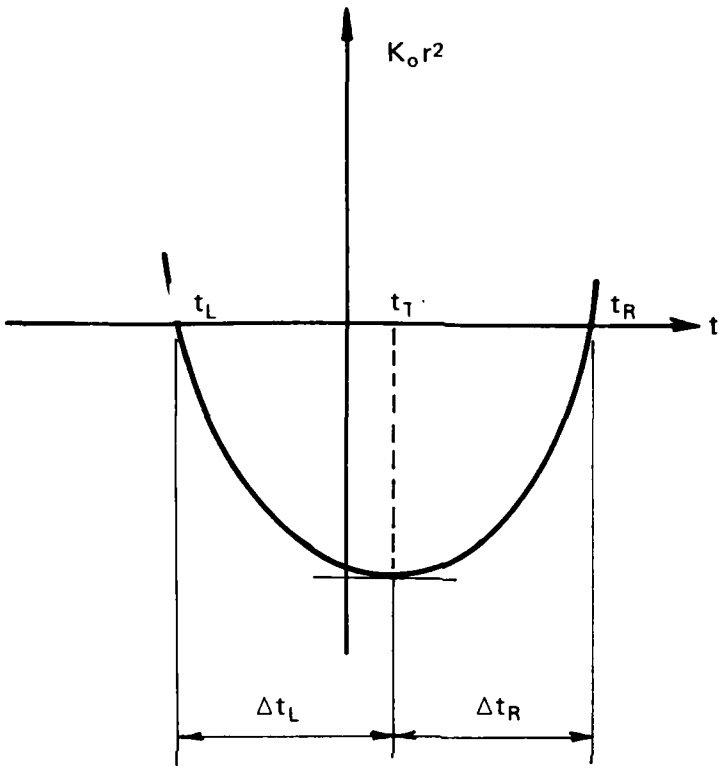

FIG. 6: DIAGRAM ILLUSTRATING THE DEFINITIONS OF Δt_L, Δt_R, t_L, t_T AND t_R IN RELATION TO THE CURVE OF $K_o r^2$.

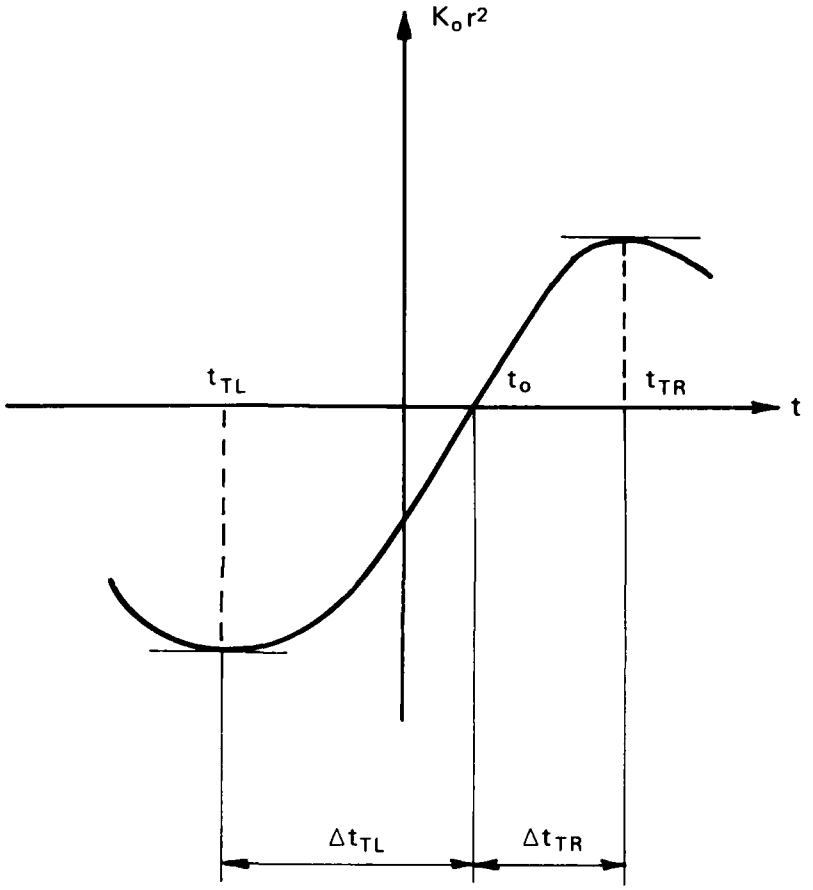

FIG. 7: DIAGRAM ILLUSTRATING THE DEFINITIONS OF Δt_{TL}, Δt_{TR}, t_{TL}, t_{TR} AND t_o IN RELATION TO THE CURVE OF $K_o r^2$ FOR PANELS THAT ARE PERPENDICULAR TO EACH OTHER.

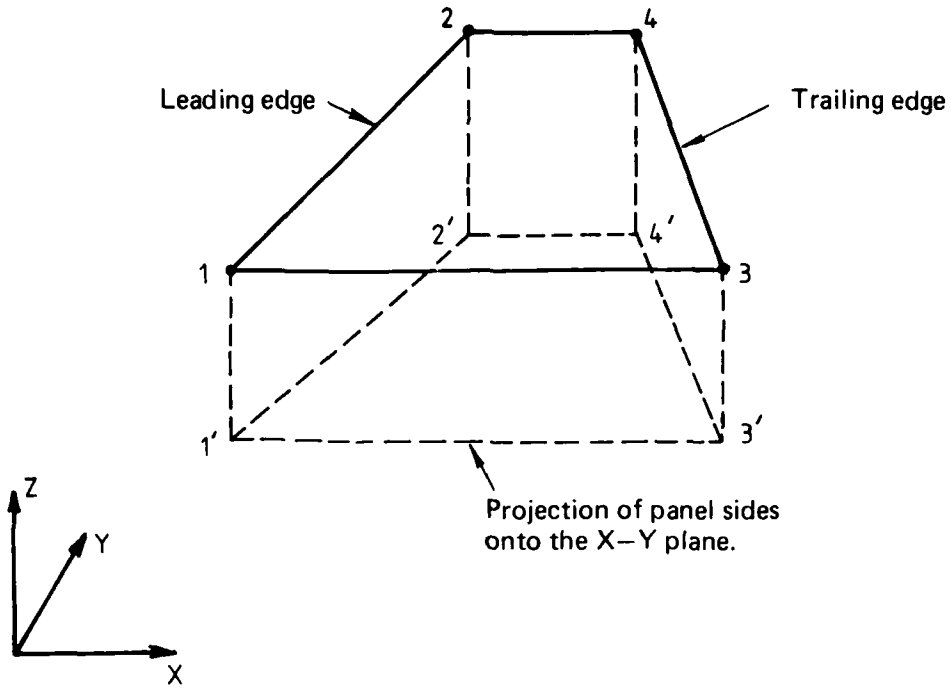

FIG. 8: DIAGRAM SHOWING NODE NUMBERING SCHEME AND OTHER FEATURES PERTAINING TO THE DEFINITION OF A GROUP. THE NUMBERS 1, 2, 3 AND 4 REFER TO THE NODES.

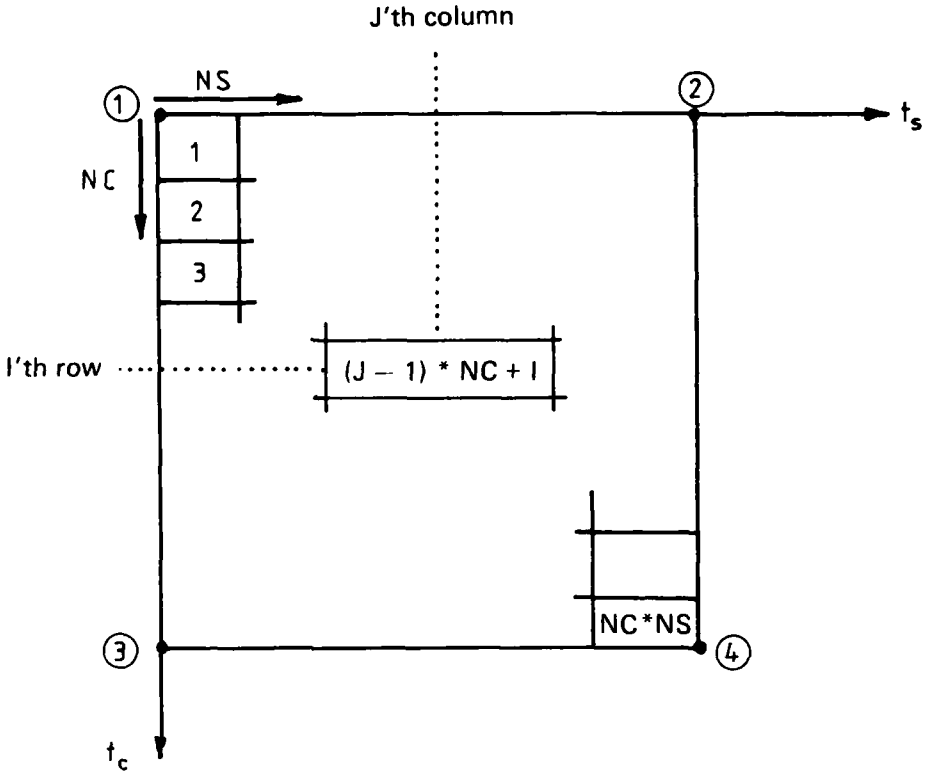

Node 1 : $(t_c, t_s) = (0, 0)$

Node 2 : $(t_c, t_s) = (0, 1)$

Node 3 : $(t_c, t_s) = (1, 0)$

Node 4 : $(t_c, t_s) = (1, 1)$

FIG. 9: DIAGRAM DEFINING NONDIMENSIONAL COORDINATE SYSTEM FOR A GROUP. ALSO SHOWN IS THE PANEL NUMBERING CONVENTION FOR PANELS WITHIN A GROUP.

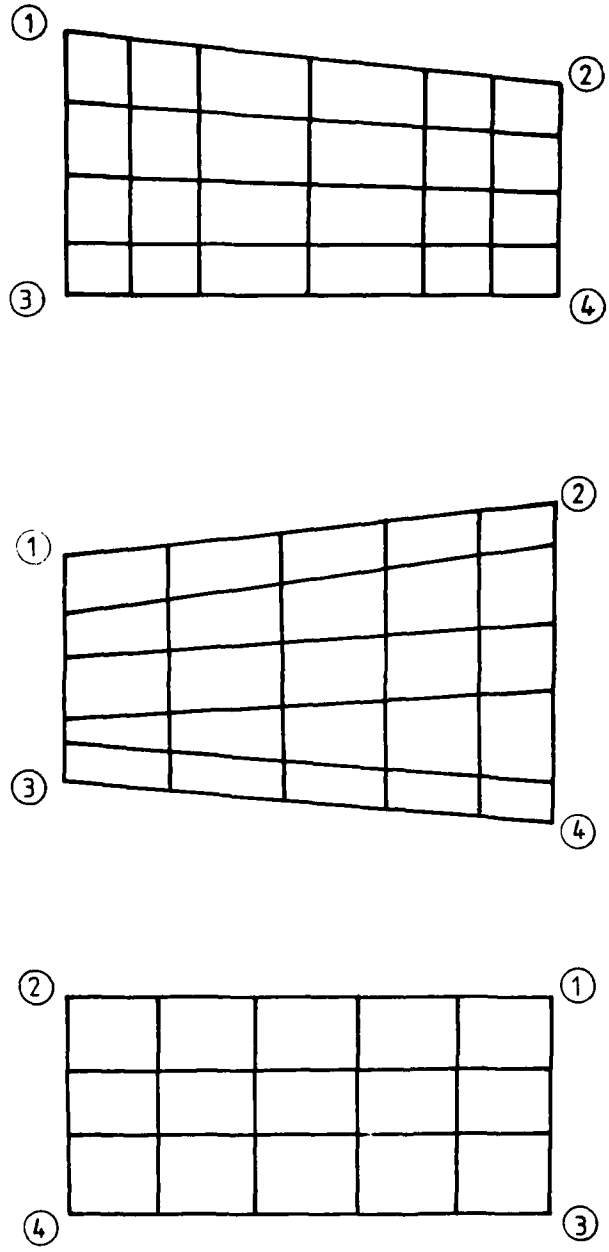

FIG. 10: DIAGRAM ILLUSTRATING SOME POSSIBLE PANEL DISTRIBUTIONS WITHIN A GROUP.

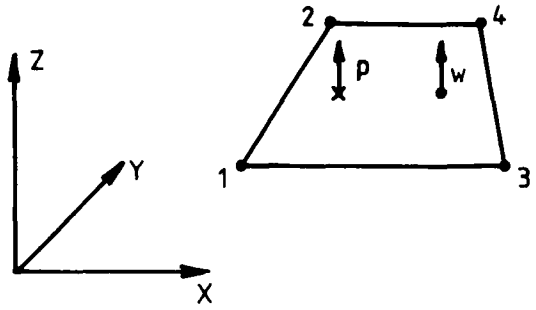

FIG. 11: DIAGRAM SHOWING POSITIVE SENSE OF PRESSURE p AND NORMALWASH w IN RELATION TO THE TOPOLOGY OF THE PANEL.

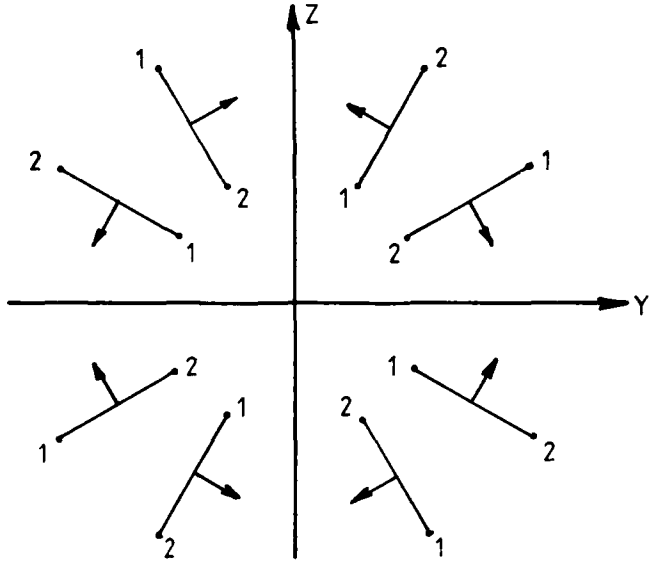

FIG. 12: DIAGRAM SHOWING POSSIBLE PANEL TOPOLOGIES IN EACH QUADRANT AND THE ASSOCIATED DIRECTION OF POSITIVE PRESSURE.

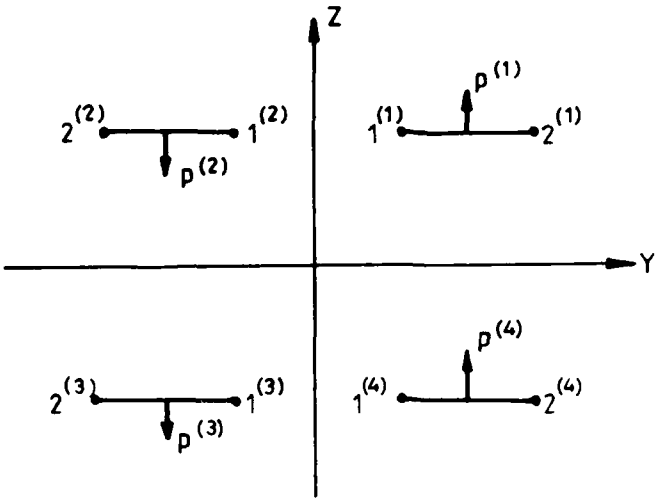

FIG. 13: TOPOLOGY OF IMAGE GROUPS, SUPERSCRIPT (2), (3) AND (4), WHEN GENERATED FROM A SOURCE GROUP (1).

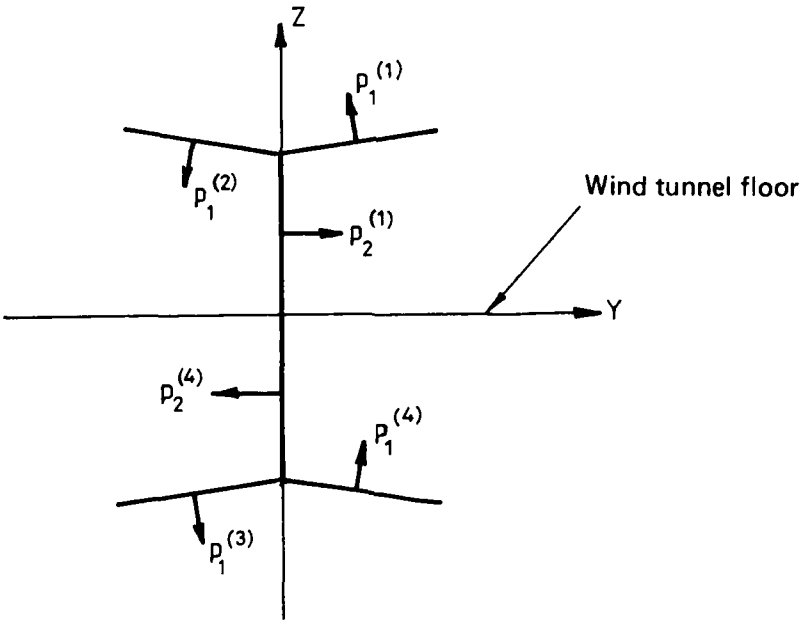

FIG. 14: IDEALISATION OF T-TAIL WITH TWO AXES OF SYMMETRY. ONLY TWO SOURCE GROUPS NEED TO BE DEFINED, THE OTHER SURFACES BEING OBTAINED BY REFLECTION. THE ARROWS INDICATE THE POSITIVE SENSES OF PRESSURE ASSUMED BY THE TOPOLOGY OF THE SOURCE GROUPS.

Tail plane is h units above plane of wing
Reference length = semi-span = 1.0

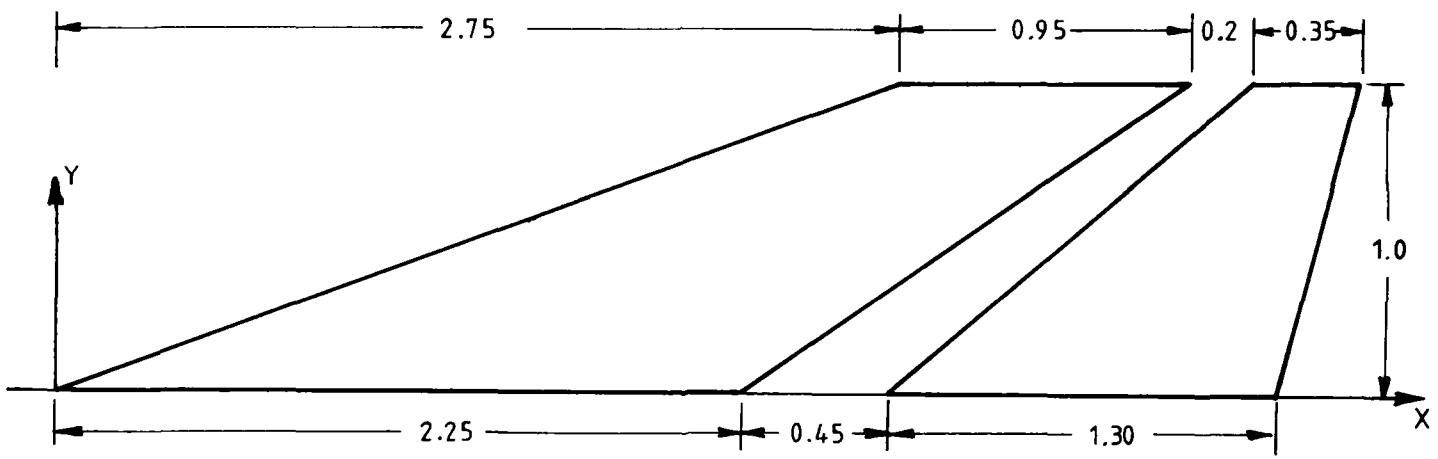

FIG. 15: AGARD HORIZONTAL WING-TAILPLANE CONFIGURATION.

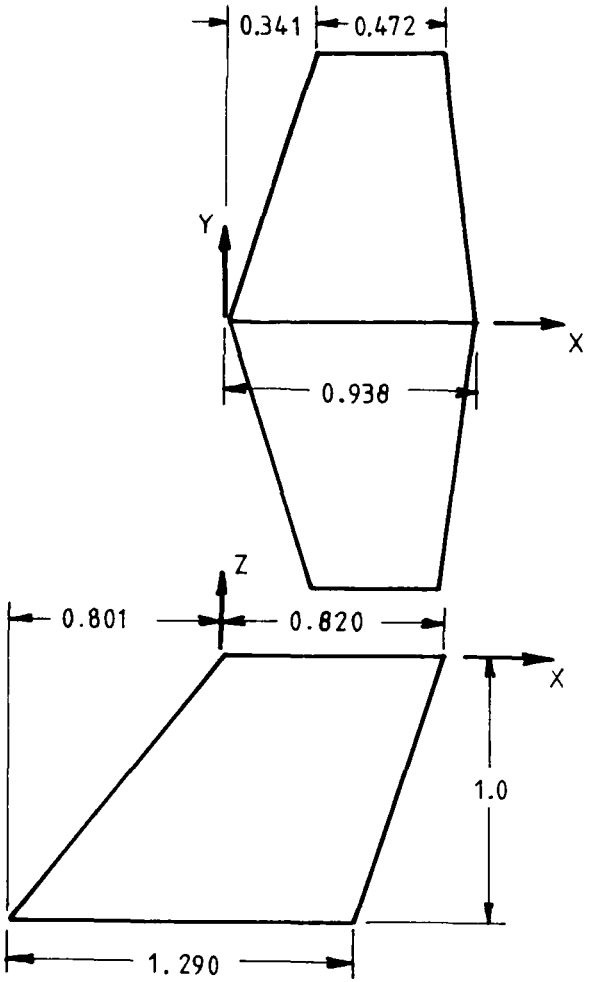

Reference length = 1.0

Mach number = 0.8

Frequency parameter = 0.0, 0.6 and 0.9

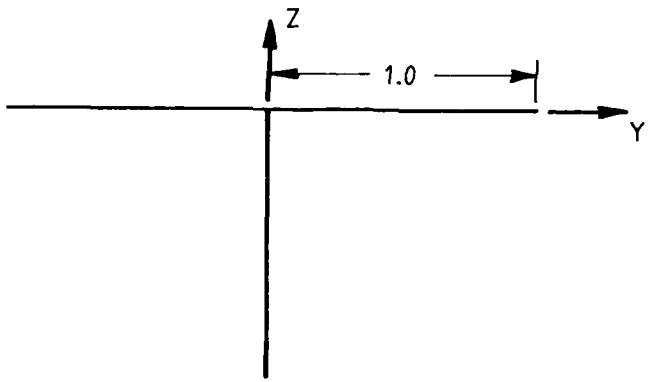

FIG. 16: STARK'S SWEPT AND TAPERED T-TAIL CONFIGURATION.

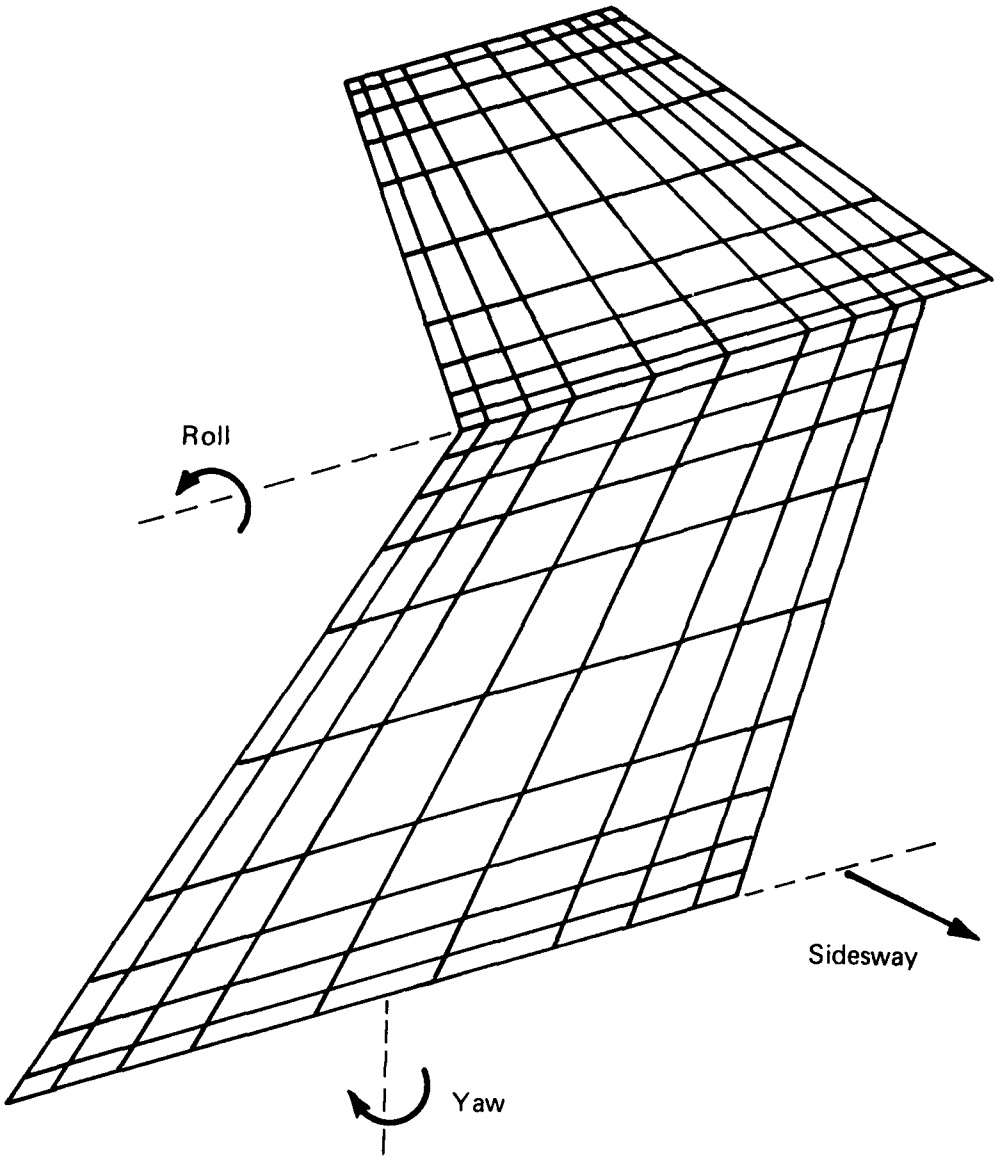

FIG. 17: PANEL DISTRIBUTION USED IN CALCULATING GENERALISED AIRFORCES FOR STARK'S T-TAIL. FOR CLARITY ONLY THE STARBOARD HALF OF THE TAILPLANE IS SHOWN.

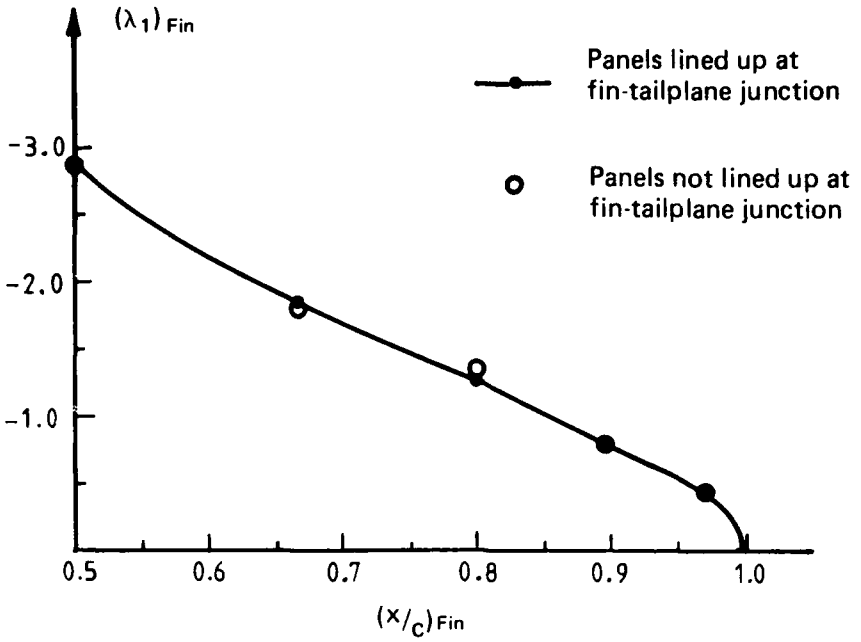

(a)

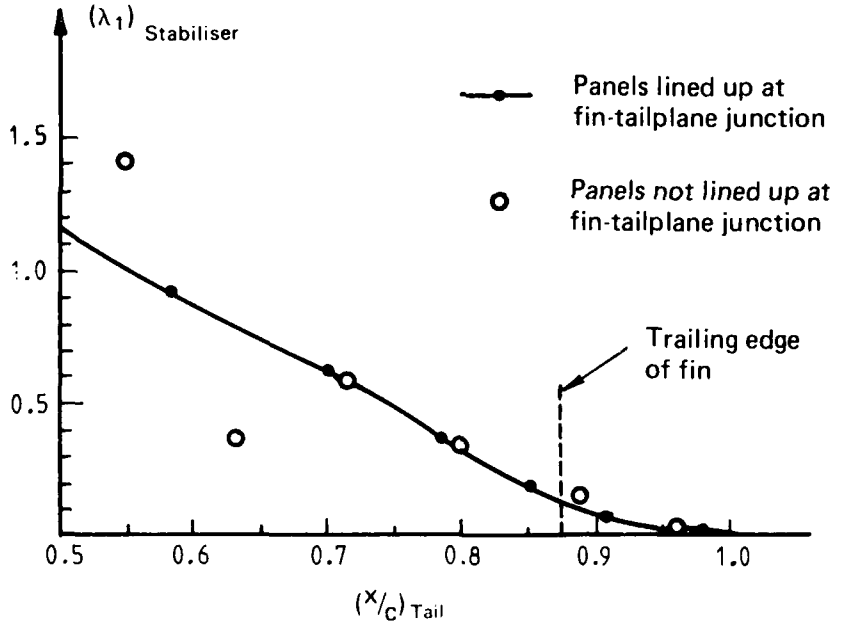

(b)

FIG. 18: PLOT OF THE NONDIMENSIONAL PRESSURE DISTRIBUTION λ_1 NEAR THE FIN-STABILISER JUNCTION FOR STARK'S T-TAIL FOR THE FIN YAW MODE (MODE F_1). PRESSURES ARE SHOWN FOR BOTH THE FIN AND STABILISER AND WERE OBTAINED FOR K = 0 & M = 0.

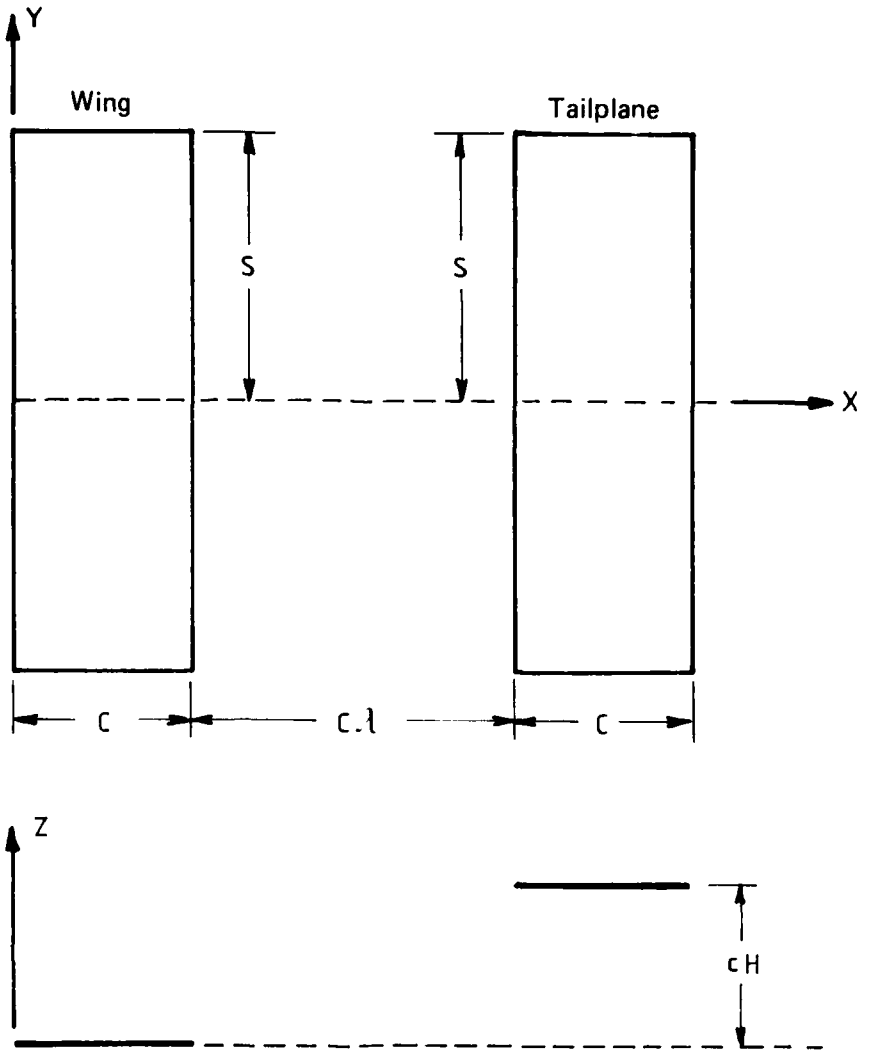

C = 0.0980 metre

S = 0.1515 metre

Reference length = C

FIG. 19: ONERA HORIZONTAL WING-TAILPLANE CONFIGURATION.

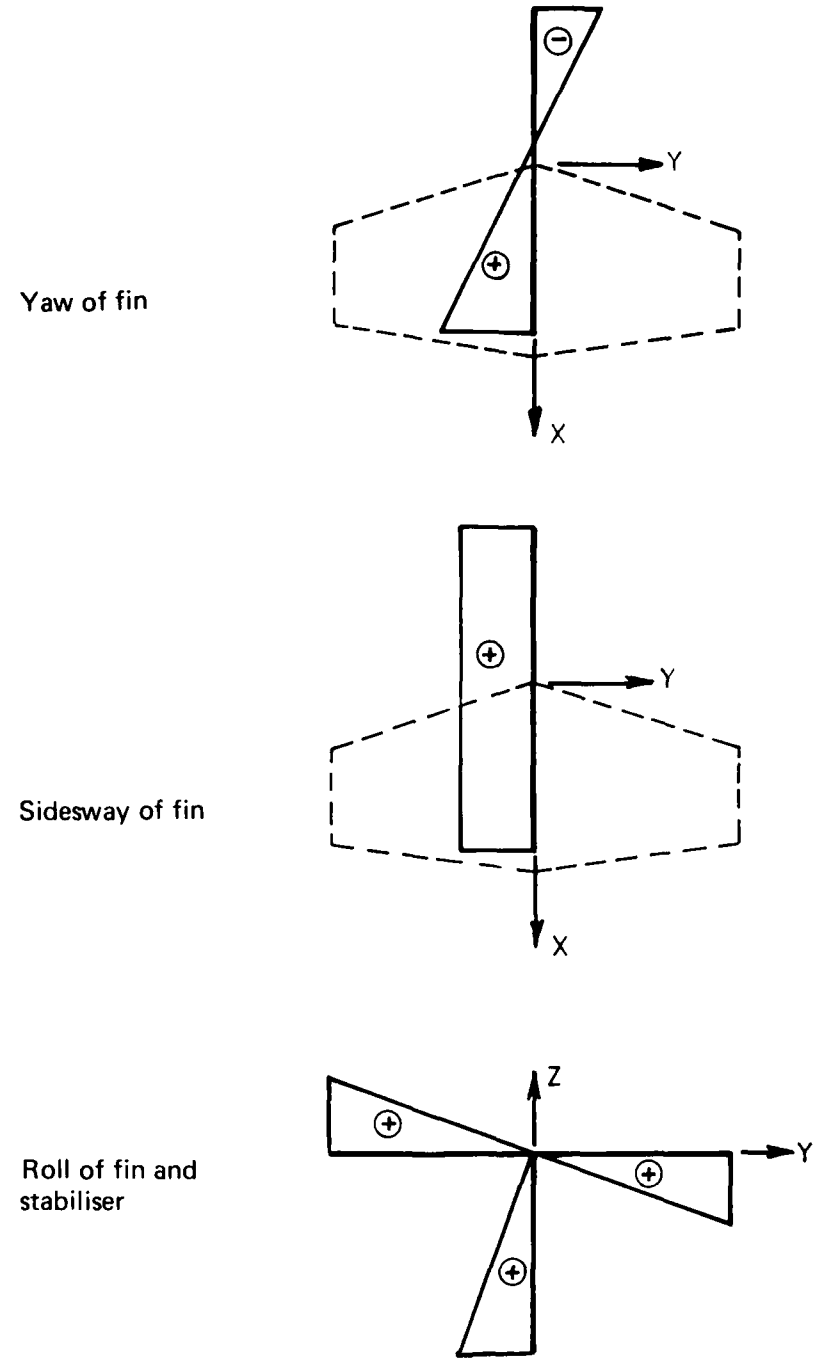

FIG. 20: SKETCH OF MODE SHAPES USED IN THE ANALYSIS OF STARK'S T-TAIL. THE + AND – SIGNS INDICATE THAT THE DISPLACEMENTS ARE IN THE SAME OR OPPOSITE DIRECTION TO THE SENSE OF POSITIVE PRESSURE FOR THE GROUP.

DISTRIBUTION

AUSTRALIA

DEPARTMENT OF DEFENCE

Central Office

Chief Defence Scientist
Deputy Chief Defence Scientist
Superintendent, Science and Program Administration
Controller, External Relations, Projects and Analytical Studies
} (1 copy)

Defence Science Adviser (UK) (Doc. Data sheet only)
Counsellor, Defence Science (USA) (Doc. Data sheet only)
Defence Science Representative (Bangkok)
Defence Central Library
Document Exchange Centre, DISB (18 copies)
Joint Intelligence Organisation
Librarian, H Block, Victoria Barracks, Melbourne
Director General—Army Development (NSO) (4 copies)

Aeronautical Research Laboratories

Director
Library
Divisional File—Structures
Author: W. Waldman
P. A. Farrell
R. Jones
B. Emslie
J. Gear

Materials Research Laboratories

Director/Library

Defence Research Centre

Library

Navy Office

Navy Scientific Adviser
RAN Aircraft Maintenance and Flight Trials Unit
Directorate of Naval Aircraft Engineering

Army Office
Scientific Adviser—Army
Engineering Development Establishment, Library
Royal Military College, Library
US Army Research, Development and Standardisation Group

Air Force Office
Air Force Scientific Adviser
Aircraft Research and Development Unit
Scientific Flight Group
Library
Technical Division Library
Director General Aircraft Engineering—Air Force
Director General Operational Requirements—Air Force
HQ Operational Command (SMAINTSO)
HQ Support Command (SLENGO)
RAAF Academy, Point Cook

Central Studies Establishment
Information Centre

DEPARTMENT OF DEFENCE SUPPORT

Government Aircraft Factories
Manager
Library
Mr W. Baird, Aerodynamics

DEPARTMENT OF AVIATION

Library
Flying Operations and Airworthiness Division

STATUTORY AND STATE AUTHORITIES AND INDUSTRY

Trans-Australia Airlines, Library
Qantas Airways Limited
Ansett Airlines of Australia, Library
Commonwealth Aircraft Corporation, Library
Hawker de Havilland Aust. Pty. Ltd., Bankstown, Library
Rolls-Royce of Australia Pty. Ltd., Mr C. G. A. Bailey

UNIVERSITIES AND COLLEGES

Adelaide	Barr Smith Library
	Professor of Mechanical Engineering
Flinders	Library
Latrobe	Library
Melbourne	Engineering Library
Monash	Hargrave Library
Newcastle	Library
Sydney	Engineering Library
NSW	Physical Sciences Library
Queensland	Library

Tasmania	Engineering Library
Western Australia	Library
	Associate Professor J. A. Cole, Mechanical Engineering
RMIT	Library
	Mr I. Herszberg, Civil & Aeronautical Engineering
	Dr L. Wood, Civil & Aeronautical Engineering

CANADA

CAARC Coordinator, Structures
International Civil Aviation Organization, Library
NRC
- Aeronautical & Mechanical Engineering, Library
- Division of Mechanical Engineering, Director
- Gas Dynamics Laboratory, Mr R. A. Tyler

Universities and Colleges

Toronto	Institute for Aerospace Studies

CZECHOSLOVAKIA

Aeronautical Research and Test Institute (Prague), Head

FRANCE

ONERA, Library

GERMANY

Fachinformationszentrum: Energie, Physic, Mathematik GMBH

INDIA

CAARC Coordinator Structures
Defence Ministry, Aero Development Establishment, Library
Gas Turbine Research Establishment, Director
Hindustan Aeronautics Ltd., Library
National Aeronautical Laboratory, Information Centre

ISRAEL

Technion-Israel Institute of Technology
- Professor J. Singer

ITALY

Professor Ing. Guiseppe Gabrielli

JAPAN

Institute of Space and Aeronautical Science, Library

Universities

Kagawa University — Professor H. Ishikawa

NETHERLANDS

National Aerospace Laboratory (NLR), Library

NEW ZEALAND

Transport Ministry, Airworthiness Branch, Library
RNZAF, Vice Consul (Defence Liaison)

Universities

Canterbury	Library
	Professor D. Stevenson, Mechanical Engineering

SWEDEN

Aeronautical Research Institute, Library
Swedish National Defence Research Institute (FOA)

SWITZERLAND

Armament Technology and Procurement Group
F + W (Swiss Federal Aircraft Factory)

UNITED KINGDOM

CAARC, Secretary
Royal Aircraft Establishment, Bedford, Library
Commonwealth Air Transport Council Secretariat
Admiralty Research Establishment, St. Leonard's Hill, Superintendent
National Gas Turbine Establishment, Director, Pyestock North
National Engineering Laboratory, Library
British Library, Lending Division
CAARC Co-ordinator, Structures
Aircraft Research Association, Library
Rolls-Royce Ltd., Aero Division, Bristol, Library
British Aerospace
  Kingston-upon-Thames, Library
  Hatfield-Chester Division, Library
Short Brothers Ltd., Technical Library

Universities and Colleges

Bristol	Engineering Library
Cambridge	Library, Engineering Department
	Whittle Library
London	Professor G. J. Hancock, Aero Engineering
Manchester	Professor, Applied Mathematics
	Professor N. Johannesen, Fluid Mechanics
Nottingham	Science Library
Southampton	Library

Liverpool	Fluid Mechanics Division, Dr J. C. Gibbings
Strathclyde	Library
Cranfield Institute of Technology	Library
Imperial College	Aeronautics Library

UNITED STATES OF AMERICA

NASA Scientific and Technical Information Facility
Applied Mechanics Reviews
The John Crerar Library
Allis Chalmers Corporation, Library
Boeing Company, Mr W. E. Binz
Kentex Research Library
United Technologies Corporation, Library
Lockheed-California Company
Lockheed Missiles and Space Company
Lockheed Georgia
McDonnell Aircraft Factory, Library

Universities and Colleges

John Hopkins	Professor S. Corrsin, Engineering
Princeton	Professor G. L. Mellor, Mechanics
Massachusetts Inst. of Technology	MIT Libraries

SPARES (10 copies)

TOTAL (155 copies)

Department of Defence

DOCUMENT CONTROL DATA

1. a. AR No.	1. b. Establishment No.	2. Document Date	3. Task No.
AR-003-987	ARL-STRUC-R-412	January, 1985	DST 82/053

4. Title	5. Security	6. No. Pages
A Fortran Program for the Determination of Unsteady Airforces on General Combinations of Interfering Lifting Surfaces Oscillating in Subsonic Flow	a. document: Unclassified b. title: U. c. abstract: U.	67 7. No. Refs: 14

8. Author(s)	9. Downgrading Instructions
W. Waldman	

10. Corporate Author and Address	11. Authority (*as appropriate*)
AERONAUTICAL RESEARCH LABORATORIES, G.P.O. Box 4331, Melbourne, Vic. 3001	a. Sponsor c. Downgrading b. Security d. Approval

12. Secondary Distribution (*of this document*)

Approved for public release

Overseas enquirers outside stated limitations should be referred through ASDIS, Defence Information Services Branch, Department of Defence, Campbell Park, CANBERRA, ACT, 2601.

13. a. This document may be ANNOUNCED in catalogues and awareness services available to . . .

No limitations

13. b. Citation for other purposes (*i.e, casual announcement*) may be (*select*) unrestricted (*or*) as for 13 a.

14. Descriptors		15. COSATI Group
Unsteady flow	Doublet lattice	01010
Subsonic flow	Panel method (fluid dynamics)	
Computer programs		
Aeroelasticity		
Aerodynamic loads		

16. Abstract

A modification of the doublet lattice method of Albano and Rodden [Ref. 1] has been programmed to calculate the unsteady generalised airforces and pressures acting on interfering lifting surfaces in subsonic flow. The present method is applicable to general nonplanar and nonparallel lifting surfaces, which may be both intersecting and nonintersecting in nature. The relevant theory is developed in detail and an outline of the program and its usage is given. Comparisons with the results of other workers are included.

This page is to be used to record information which is required by the Establishment for its own use but which will not be added to the DISTIS data base unless specifically requested.

16. Abstract (*Contd*)

17. Imprint

Aeronautical Research Laboratories, Melbourne

18. Document Series and Number	19. Cost Code	20. Type of Report and Period Covered
Structures Report 412	236925	—

21. Computer Programs Used

—

22. Establishment File Ref(s)

—

DTIC

FILMED

4-86

END